Intra-epithelial non-canonical Activin A signalling safeguards prostate progenitor quiescence

Francesco Cambuli[1,3,#,*,δ], Veronica Foletto[1,#], Alessandro Alaimo[1], Dario De Felice[1], Francesco Gandolfi[2], Maria Dilia Palumbieri[1], Michela Zaffagni[1], Sacha Genovesi[1], Marco Lorenzoni[1], Martina Celotti[1], Emiliana Bertossio[1], Giosuè Mazzero[4], Arianna Bertossi[1], Alessandra Bisio[1], Francesco Berardinelli[5,6], Antonio Antoccia[5], Marco Gaspari[7], Mattia Barbareschi[4], Michelangelo Fiorentino[8], Michael M. Shen[3], Massimo Loda[9], Alessandro Romanel[2], and Andrea Lunardi[1,*].

[1]The Armenise-Harvard Laboratory of Cancer Biology & Genetics, Department of Cellular, Computational and Integrative Biology (CIBIO), University of Trento, 38123 Trento (TN), Italy.

[2]Laboratory of Bioinformatics and Computational Genomics, Department of Cellular, Computational and Integrative Biology (CIBIO), University of Trento, 38123 Trento (TN), Italy.

[3]Department of Medicine, Genetics and Development, Urology, Systems Biology, Herbert Irving Comprehensive Cancer Center, Columbia University Irving Medical Center, New York, NY 10032, USA.

[4]Santa Chiara Hospital-APSS, Trento, 38122 Trento (TN), Italy.

[5]Department of Science, University of Roma Tre, 00146 Roma, Italy.

[6]Laboratory of Neurodevelopment, Neurogenetics and Molecular Neurobiology Unit, IRCCS Santa Lucia Foundation, 00143, Rome, Italy

[7]Department of Experimental and Clinical Medicine, University of Catanzaro, 88100 Catanzaro (CZ), Italy.

[8]Department of Experimental, Diagnostic and Specialty Medicine, University of Bologna, 40138 Bologna (BO), Italy.

[9]Department of Pathology and Laboratory Medicine, Weill Medical College of Cornell University, New York, NY10021, USA.

[#] These authors contributed equally as first authors

* Corresponding author: +1 646 888 3997 cambulif@mskcc.org

* Corresponding author: +39 0461 285288 andrea.lunardi@unitn.it

[δ] Present address: Molecular Pharmacology Program, Sloan Kettering Institute, Memorial Sloan Kettering Cancer Center, New York, NY 10065, USA

Keywords

Activin A / Organoids / P38-MAPK/ Prostate / TGF-β

Abstract

The healthy prostate is a relatively quiescent tissue. Yet, prostate epithelium overgrowth is a common condition during ageing, associated with urinary dysfunction and tumorigenesis. For over thirty years, TGF-β ligands have been known to induce cytostasis in a large variety of epithelia, but the intracellular pathway mediating this signal in the prostate, as well as its relevance for quiescence, have remained elusive.

Here, using mouse prostate organoids to model epithelial progenitors, we found that intra-epithelial non-canonical Activin A signalling inhibited cell proliferation in a Smad-independent manner. Mechanistically, Activin A triggered Tak1 and p38 MAPK activity, leading to p16 and p21 nuclear import. Spontaneous evasion from this quiescent state occurred upon prolonged culture, due to reduced Activin A secretion, a condition associated with DNA replication stress and aneuploidy. Organoids capable to escape quiescence *in vitro* were also able to implant with increased frequency into immunocompetent mice.

Our study demonstrates that non-canonical Activin A signalling safeguards epithelial quiescence in the healthy prostate, with potential implications for the understanding of cancer initiation, and the development of therapies targeting quiescent tumour progenitors.

57 **Introduction**

58 The healthy prostate is a relatively quiescent tissue during adulthood[1,2]. In contrast, the overgrowth
59 of the prostatic epithelium is one of the most common conditions experienced by ageing men, being
60 linked with urinary dysfunction and tumorigenesis[3]. The molecular mechanisms causing exit from
61 quiescence are poorly understood. Chronic inflammation – potentially induced by infection (*e.g.,*
62 prostatitis)[4–6], chemical damage (*e.g.,* urine reflux)[7], physical trauma (e.*g.,* corpora amylacea)[8],
63 dietary carcinogens[9], obesity[10], hormonal imbalance (*e.g.*, low systemic androgen levels)[11,12], and
64 ageing[13] – has been implicated in DNA damage, oxidative stress, and atrophy, leading to a
65 proliferative response[14,15]. Considering the high frequency of these events, it would be logical to
66 hypothesize specialized mechanisms to safeguard epithelial quiescence, but they have been rarely
67 investigated.

68 It has long been known that Transforming Growth Factor β (TGF-β) signalling inhibits the
69 proliferation of a large variety of epithelial cell types[16,17], including those of the prostate[18]. SMAD
70 factors are the canonical intracellular mediators of this signalling, but additional non-canonical
71 pathways can also be triggered by TGF-β receptors[19,20]. In gastrointestinal (GI) carcinomas (*e.g.*,
72 pancreas, colon), the canonical pathway is frequently mutated[21,22]. However, outside of the GI tract,
73 TGF-β/SMAD components are rarely inactivated in tumours, leaving unexplained the nature of the
74 intracellular signalling responsible for the cytostatic effect of TGF-β[23,24].

75 Enhanced Tgf-β signalling has been linked with the presence of quiescent epithelial
76 progenitors in the proximal/periurethral region of the mouse prostate[25,26]. Recent single-cell studies
77 have confirmed the enrichment of a variety of epithelial progenitors – basal, luminal proximal
78 (LumP), and periurethral (PrU) cells – in this anatomical district, though also present at low frequency
79 in the distal compartment[27–32]. Such cells are known to be particularly quiescent during
80 homeostasis[33,34], but also to exhibit extensive regenerative potential in *ex-vivo* assays[31,35].

81 Thus, the TGF-β induced cytostatic response in epithelial progenitors may be relevant for the
82 control of quiescence, but the complexity of this pathway, the lack of interpretable genetic alterations
83 in patients, and the heterogeneous cellular composition of the prostate, have so far hampered
84 mechanistic investigations. Here, we reasoned that prostate organoid models[36,37] – in combination
85 with orthotopic transplantation approaches – may provide a biologically relevant, and experimentally
86 amenable, system for addressing this question.

87

Results

Mouse prostate organoid cultures enable the continuous expansion of epithelial progenitors in a near-physiological manner.

Initially, we set out to assess whether mouse prostate organoids are a representative and informative model for the study of the prostate epithelium, in light of recent discoveries on prostate cellular heterogeneity and dynamics[27,28,30–32,34,38]. Considering our interest in signalling, we focused on a culture method in defined media conditions. This protocol relies on a mix of growth factors and inhibitors, including Egf, Noggin, R-spondin 1, the Tgf-β receptors inhibitor A83-01, and dihydrotestosterone (ENRAD)[36]. We generated a biobank of mouse prostate organoids, starting from bulk populations of cells from distinct prostate lobes and mouse strains (Fig. 1a, Supplementary Fig S1). In line with previous studies[36,37], we found that, upon tissue dissociation, only a small fraction of cells (approx. 1%) was capable to generate organoids in culture, and that organoid-forming efficiency increased over passages, suggesting enrichment for epithelial progenitors (Fig. 1b). To gain greater insights, we longitudinally tracked organoid formation – from single cells to fully formed organoids – and we observed a progressive expansion of cells expressing the progenitor epithelial surface antigen Sca-1 (encoded by *Ly6a*) (Fig. 1c)[31,35]. Thereafter, the level of Sca-1 appeared to be stable over a long culture period (*e.g.*, 10 weeks). To extend our observations, we performed transcriptomic analyses on three organoid lines derived from distinct mouse prostate lobes (Fig. 1d,e). Consistently with enrichment for epithelial progenitors, organoids expressed high levels of genes specific for the proximal and periurethral compartments (*e.g.*, *Psca*, *Tacstd2*, and *Ly6d*), as well as basal (*e.g.*, *Krt5*, *Krt14, Trp63*) and luminal marker genes (*e.g., Krt8*, *Ar, Foxa1*). In contrast, distal luminal markers were barely detectable (*e.g., Nkx3.1*, *Pbsn*, *Sbp*). Histological (H&E) and immunofluorescent (IF) analyses confirmed that prostate organoids, for the most part, are made up of a bilayer of cuboidal cells, displaying progenitor marker proteins (*e.g.*, Krt7, Ppp1r1b), and resembling the cyto-architecture of the periurethral/proximal compartment (Fig. 1f-h). As expected for periurethral/proximal cells – which are known to be castration resistant – mouse prostate organoids were reversibly dependent on androgen for lumen formation, but not for their survival (Supplementary Fig. S2).

The epithelium of the prostate is characterized by a slow cellular turnover. In contrast, prostate organoids appeared to proliferate indefinitely – while retaining low levels of genomic instability (Supplementary Fig. S3) – raising the question of how culture conditions enable persistent cycling in a near-physiological manner. Either an excess of stimulatory cues in culture, or a lack of inhibitory

120 ones – or both – may explain the shift from homeostatic quiescence *in vivo* to unrestrained mitotic
121 activity *in vitro*. Using a 'n -1 approach' for assessing the requirement for growth factors and
122 inhibitors in culture (Supplementary Fig. S4a), we found that prostate organoids are strictly dependent
123 on Egf, with sub-nanogram concentration levels being sufficient for cell cycle progression
124 (Supplementary Fig. S4b,c). Still – based on ligand/receptor expression patterns – Egf signalling
125 alone is unlikely to explain the excess of proliferation in culture. Indeed, *Egf* is highly transcribed by
126 distal luminal cells in the adult prostate[28], and progenitor cells express the Egf receptor *in vivo* –
127 independently of their proximal or distal location – at levels comparable to those observed *in vitro*
128 (Supplementary Fig. S4d). Therefore, we focused on the requirement for the Tgf-β receptor inhibitor
129 A83-01 for the continuous expansion of mouse prostate organoid cultures.

130 **Intra-epithelial non-canonical Activin A signalling is a key mediator of the Tgf-β induced**
131 **cytostatic response in mouse prostate organoids.**

132 Upon A83-01 withdrawal, organoids displayed a marked reduction in EdU incorporation
133 within 24 hours, demonstrating a cytostatic response in this model (Fig. 2a, Supplementary Fig. S5a).
134 A83-01 is a potent inhibitor of three type-I Tgf-β family receptors, and two of them - Acvr1b and
135 Tgfbr1 (also known as Alk4 and Alk5) – were found to be expressed in prostate organoids
136 (Supplementary Fig. S5b). Paracrine and autocrine ligand-receptor interactions have been
137 demonstrated to negatively regulate epithelial proliferation[16,39] leading us to investigate the release
138 of Tgf-β ligands in organoid cultures. We employed a click-chemistry approach to enrich for secreted
139 proteins released in the culture medium, followed by mass-spectrometry analysis[40]. Over multiple
140 experiments, we consistently recovered Activin A peptides (encoded by the *Inhba* gene) in the
141 organoid supernatant, and only in one instance, a Tgfb1 peptide (Fig. 2b). We were also able to
142 immunolocalize Acvr1b in organoid cells, and in progenitor cells *in vivo* (Fig. 2c), with an expression
143 pattern similar to Egfr (Supplementary Fig. S4d). Replacement of A83-01 with Follistatin - a well-
144 known Activin A inhibitor[41] – was sufficient to sustain proliferation, revealing a prominent role for
145 the latter in inducing a cytostatic response (Fig. 2d). To gain greater insights on the downstream
146 pathway, we boosted Tgf-β receptor activity by combining A83-01 withdrawal with the
147 supplementation of distinct ligands. Activin A was found to enhance the non-canonical arm of Tgf-β
148 signalling – mediated by the Tgf−β activated kinase, Tak1 (encoded by the *Map3k7* gene), and the
149 downstream p38 MAPKs – as well as the accumulation of the cell cycle inhibitor p21 (Fig. 2e). In
150 contrast, Tgfb1 increased the activity of the canonical Tgf-β pathway – via Smad2/3 phosphorylation,
151 but with little, if any, alteration of p21 levels. This dichotomy prompted us to functionally test the

152 role of the canonical, and non-canonical pathway, respectively. Disruption of the canonical pathway,
153 via shRNA-mediated silencing of Smad4, did not alter the cytostatic response upon A83-01
154 withdrawal (Supplementary Fig. S6). In contrast, the inhibition of either Tak1 or the structurally
155 related p38α and p38β MAPKs – using a variety of inhibitors (Fig. 2f,g; Supplementary Fig. S7a,b)
156 – was sufficient to ensure organoid expansion in the absence of Tgf-β receptor blockade.

157 TGF-β receptors, and cytokine-stimulated receptors (*e.g.*, IL-1, TNF, type-I interferons), are
158 known to converge on TAK1-p38 MAPK signalling to activate a variety of downstream factors
159 controlling immune- and stress-related responses, including well-characterized transcriptional
160 programmes[42–45]. By combining bulk-RNA sequencing and biochemical approaches, we confirmed
161 that in the absence of Tgf-β receptors inhibition, Tak1-p38α/β signalling resulted in phosphorylation
162 and nuclear shuttling of immune-related transcription factors (*e.g.*, Stat1/2, NF-kB), which led to the
163 transcription of immune related gene sets (*e.g.,* induced by TNF or type-I interferons)[46], as well as to
164 the phosphorylation of the stress-related kinase Mapkapk2 (Fig. 2h,i; Supplementary Fig. S7c-f).
165 Importantly, Tak1-p38 MAPK activity was associated with the nuclear accumulation of the key cell
166 cycle inhibitors p21 and p16 (Fig. 2h).

167 Collectively, our data demonstrated that intra-epithelial non-canonical Activin A signalling
168 induce a cytostatic response in mouse prostate organoids.

169 **Evasion from the Tgf–β induced cytostatic response via downregulation of intra-epithelial**
170 **Activin A signalling.**

171 We reasoned that our biobank may offer the opportunity to discover mechanisms of evasion
172 from the Tgf–β induced cytostatic response, mediated by intra-epithelial Activin A signalling, in an
173 unbiased manner. Therefore, we attempted to culture multiple prostate organoid lines in the absence
174 of A83-01, waiting for the potential emergence of clones capable to thrive in these conditions. Out of
175 nine prostate organoid lines (from three distinct mice), six were irreversibly lost within few weeks.
176 Still, three lines survived for an extended period, with two of them eventually adapting to the absence
177 of A83-01 and recovering the ability to be passaged at clonal density (Fig. 3a,b; Supplementary Fig.
178 S8). We performed bulk-RNA sequencing on the C57#1 DLP organoid line in the presence of A83-
179 01, one day after inhibitor withdrawal, and upon adaptation; additionally, we sequenced the C57#3
180 DLP organoid line in control conditions and following adaptation (Fig. 3c). We focused on
181 transcriptional alterations shared by both lines displaying adaptation to A83-01 withdrawal. First, we
182 noticed that gene signatures associated with ATR signalling were strongly upregulated upon

183 adaptation (Fig. 3d), indicating potential DNA replication stress in S-phase, a finding consistent with
184 phosphorylation of the cell cycle Checkpoint kinase 1 (Chek1) (Fig. 3e). Of note, in the adapted
185 C57#1 DLP line we detected widespread genomic instability and telomere doublets, a hallmark of
186 DNA replication stress, while retaining an intact p53 pathway (Fig. 3f-h; Supplementary Fig. S9).
187 Second, in both adapted organoid lines, we observed the downregulation of immune-related
188 transcriptional programmes (*e.g.*, type-I interferon stimulated genes), suggesting an impairment of
189 non-canonical Activin A signalling (Supplementary Fig. S10). Consistently, we found that adapted
190 organoid lines significantly reduced Activin A secretion in culture (Fig. 3i), and that exogenous
191 Activin A (but not Tgfb1) was sufficient to restore the cytostatic response (Fig. 3j,k; Supplementary
192 Fig. S11).

193 Thus, mouse prostate organoids are capable to dampen the Tgf-β induced cytostatic response
194 by downregulation of intra-epithelial Activin A signalling.

195 **Mouse prostate organoids with reduced intra-epithelial Activin A signalling display enhanced**
196 **engraftment upon syngeneic transplantation.**

197 We wondered whether a reduced intra-epithelial Activin A signalling may release the
198 progenitor proliferative potential in response to basal growth stimuli, within the relative quiescent
199 microenvironment of the adult prostate epithelium. To test this hypothesis, we orthotopically
200 transplanted dissociated mouse prostate organoid cells into immunocompetent syngeneic mice (Fig.
201 4a). Donor cells were injected into the extensive branchial structures of the distal anterior prostate, to
202 avoid damage to the delicate proximal ducts, and maximize the probability of retention. Implantation
203 of donor cells into an immunocompetent host tissue characterized by a slow turnover can be
204 considered challenging. Still, we found that, in comparison to control organoid cells, organoid cells
205 adapted to grow without A83-01 implanted with high frequency (Fig. 4b), and gave rise to dysplastic
206 foci, characterized by elevated mitotic index, cuboidal histology and nuclear atypia (Fig. 4c,d).

207 We conclude that intra-epithelial non-canonical Activin A signalling safeguards quiescence
208 in prostate progenitors.

209 Discussion

210 Signalling pathways ensure coordination of tissue development, homeostasis, regeneration,
211 and their disruption can lead to disease. The molecular bases of specific signals are difficult to
212 investigate, due to the challenges of disentangling cellular cross talks *in vivo*, and of establishing
213 representative models *in vitro*. More recently, organoid models in defined media conditions have

214 opened new opportunities for the study of epithelia[47]. Benchmarking of these models with their
215 corresponding *in vivo* counterpart is paramount for the correct experimental interpretations[48]. Here,
216 we demonstrated that mouse prostate organoid cultures enable the continuous expansion of epithelial
217 progenitors *in vitro*, including basal, LumP and PrU cells. Such cell types are predominantly found
218 near the urethra *in vivo*, but also in the distal prostate compartment at low frequency. Our work
219 revealed that progenitor proliferation is dynamically regulated by the antagonistic equilibrium
220 between Egf and non-canonical Activin A signalling, respectively – with at least partial reduction of
221 the latter required for cell cycle progression. The rationale perturbation of additional biochemical
222 signals, and mechanical cues, may enhance progenitor differentiation towards distal luminal cells in
223 culture.

224 It has long been known that the broad family of TGF-β signals induces a cytostatic response
225 in a large variety of epithelial cells, but the specific pathway acting in the prostate has remained
226 poorly understood. Earlier studies pointed to the importance of the Tgf-β family ligand Activin[49,50].
227 At the mechanistic level, DePinho and colleagues initially focused on the role of Smad4 as a
228 proliferative barrier in a *Pten*-loss driven mouse model of prostate cancer[51]. Follow-up studies from
229 the same group and others, carried out in humans and mice, have led to a more complex view[52,53],
230 with the involvement of both canonical and non-canonical pathways.

231 We propose a prominent role for non-canonical Activin A signalling in safeguarding
232 quiescence in prostate epithelial progenitors (Fig. 4e). Our model may be relevant beyond tissue
233 homeostasis and the response to inflammation. Genes encoding for core components of the non-
234 canonical Activin A signalling pathway (*e.g.*, *ACVR2A, MAP3K7*) are frequently lost in prostate
235 cancer, based on large cohorts of patients in the U.S.A.[54] and in China[55]. Moreover, *MAP3K7* loss
236 has been linked to genomic instability in human prostate cancer cell lines[56] and found to promote an
237 aggressive transcriptional programme in prostate tumours, based on a recent systematic pan-cancer
238 analysis[57]. In contrast, genetic alterations rarely affect TGFB1 receptors (*e.g.*, *TGFBR2*) or SMAD
239 factors (*e.g., SMAD4*), and enhanced canonical TGF-β signalling has been reported in metastatic
240 biopsies in therapy-resistant prostate cancer patients[58]. We speculate that loss of the non-canonical
241 TGF-β arm could impair the cytostatic response, while sparing the well-known transforming potential
242 of the TGF-β canonical pathway.

243 Tak1/p38-MAPK signalling stimulated two main sets of effector proteins in prostate
244 progenitors. On the one hand, we observed the nuclear translocation of key negative cell cycle
245 regulators (*e.g.*, p16 and p21). On the other hand, using biochemical and transcriptional analyses, we
246 demonstrated the activation of a broad transcriptional response, reminiscent of those induced by

247 inflammatory cytokines and pathogens. These findings are in line with recent observations on the
248 immune function of structural cells[59] and suggest a cross talk between the epithelial and immune
249 compartments, beyond the well-known mechanisms of anti-microbial defence. Prostate progenitors
250 – and, perhaps, other types of epithelia cells – may have the ability to signal changes in their
251 proliferative status and, immune cells may have the capability to adjust their function in response.

252 To test the relevance of intra-epithelial non-canonical Activin A signalling for the
253 enforcement of quiescence in prostate progenitors, we performed experiments *in vitro* and *in vivo*.
254 Our long-term organoid cultures – in the absence of Tgf-β receptor blockade – revealed that cells
255 capable to re-enter cell cycle had downregulated Activin A secretion. Moreover, those cells were also
256 capable to implant and proliferate at increased frequency *in vivo*. While stromal sources of Tgf-β
257 ligands have been previously described in the prostate[25,26], our study is the first to demonstrate a key
258 role for intra-epithelial signalling.

259 Notably, dysregulation of non-canonical Activin A signalling was associated to DNA
260 replication stress and genomic instability, a finding that may be relevant for tumour initiation. Indeed,
261 distal LumP cells have been shown to serve as cell-of-origin for prostate cancer[30]. In this regard, our
262 orthotopic transplantation approach may be particularly relevant for investigating the tumorigenic
263 potential of distal progenitor cells.

264 Finally, P38 MAPK inhibitors – including Ralimetinib – are currently being tested in phase
265 1/2 clinical trials[60]. Quiescent tumour progenitors – induced by the broad family of TGF-β signals -
266 are emerging as key mediators of chemotherapy resistance in solid malignancy[61]. In advanced
267 prostate cancers with a genetically intact Activin A non-canonical pathway, P38 MAPK inhibitors
268 may force tumours progenitors out of quiescence, improving the efficacy of standard chemotherapy
269 regimens[62]. While the complexity and pleiotropy of TGF-β signalling has historically complicated
270 drug development[63], the elucidation of cell- and context-specific pathways may lead to novel
271 therapeutic opportunities.

272 Methods

273 Mice.

274 Animal experiments were performed according to the European Communities Council Directive
275 (2010/63/EU) and approved by the Italian Ministry of Health and the University of Trento Animal
276 Welfare Committee (642/2017-PR). Wild-type C57BL/6J (JAX # 000664) mice were purchased from
277 the Jackson Laboratory. Wild-type BALB/c (CRL # 028) and CD-1 (CRL # 022) mouse strains were
278 obtained from the Charles River Laboratories.

279 **Isolation of mouse prostate tissue.**
280 The anterior (AP), dorso-lateral (DLP) and ventral prostate (VP) lobes were dissected individually,
281 using a transverse cut at the intersection of each lobe with the urethra. Paired lobes were collected for
282 organoid cultures, histology and immunostaining studies.
283 **Dissociation of mouse prostate tissue to single cells**.
284 Prostate tissue was minced into small pieces, washed, resuspended into a digestion buffer -including
285 Collagenase II (1 mg/mL; Life Tech, 17101015) and Dispase II (10 mg/mL; Life Tech 17105041),
286 and transferred into a gentleMACS C tube (Miltenyi Biotec). Tissue fragments were processed by
287 alternating mechanical disruption - using the gentleMACS Dissociator (A.01 -C tube programme) –
288 and enzymatic digestion -incubating the solution at 37 °C on a tube rotator for 15 minutes. After three
289 cycles, the cell suspension was pelleted, resuspended in TrypLE (Life Tech, 12605010), and
290 incubated for 5 minutes at 37 °C. After two washes, the cell suspension was filtered through a 70 µm
291 strainer and counted.
292 **3D prostate organoid cultures.**
293 Dissociated prostate cells were resuspended in 80% growth factor-reduced basement matrix (either
294 Matrigel®,Corning, 356231; or BME-2®,AMSBIO, 3533) and seeded at the concentration of
295 approximately 50,000 cells/mL, by depositing at least six 40 µL drops at the bottom of a non-tissue
296 culture treated plate. Basement matrix domes were left to solidify for 15 minutes and covered with
297 ENRAD medium – including Egf (50 ng/mL; PeproTech, 315-09), Noggin (100 ng/mL; PeproTech,
298 120-10C), R-Spondin1 (10% conditioned medium), A83-01 (200 nM; Tocris, 2393) and
299 dihydrotestosterone (10 nM; Merck, 10300) – supplemented with Y-27632 (10 µM; Calbiochem,
300 146986-50-7), as previously described[64]. Organoids were cultured in a standard tissue culture
301 incubator, with medium replacement every 2-3 days. After 6 days from the initial seeding, organoids
302 were imaged with a Leica MZ16F stereomicroscope and organoid forming efficiency was calculated.
303 For subsequent passages, the basement membrane was dissolved using a recovery solution –
304 including Dispase II (1 mg/mL) – and organoids were dissociated to small clumps/single cells as
305 described above, using TrypLE. Following the first passage, organoids were seeded at the
306 concentration of approximately 25,000 cells/mL.
307 **Lentiviral transduction of organoids.**
308 Organoids were dissociated to single cells, and approximately 50,000 cells were transduced for each
309 condition. Spinoculation was performed in a low-adhesion 96 well-plate using 0.6 RTU of lentiviral
310 solution, supplemented with polybrene (4 µg/mL; Sigma Aldrich, H9268) and complete medium
311 (ENRAD) to reach a final reaction volume of 300 µL. The plate was sealed with parafilm and

312 centrifuged for 1 hour at 600 g. Afterwards, the cells were resuspended in 200 µL of complete medium
313 (ENRAD), supplemented with Y-27632 (10 µM), and incubated in suspension at 37 °C for 4-6 hour.
314 After centrifugation, the cell pellet was resuspended in 80% basement matrix and seeded as described
315 above. Antibiotic selection was initiated two days post-transduction. The following plasmids were
316 used: pLenti-AIB-EGFP (kindly donated by Massimo Pizzato), pSUPER-retro-puro-Smad4
317 (Addgene #89829) and pSUPER-retro-puro-GFP shRNA (Addgene #30519).
318 **Treatments with growth factors and small molecule inhibitors.**
319 Growth factors and small molecules used in this study are described in Supplementary Table 1.
320 **Flow cytometry.**
321 Organoids were dissociated to single cells as described above. For cell surface antigen expression
322 analysis, cells were incubated with anti-Cd24a-APC and Sca-1-PE-Cy7 antibodies (1:800 dilution) at
323 4°C for 20-30 minutes, followed by one wash with FACS buffer (1% FBS, 1mM EDTA). Cells were
324 resuspended in FACS buffer, supplemented with 1 µM propidium iodide (Life Tech, P3566) for dead
325 cell exclusion, before proceeding to the analysis. For DNA content analysis, cells were resuspended
326 in 100 µl ice-cold PBS and transferred to a 15 ml tube. About 900 µl of ice-cold EtOH 70% were
327 added dropwise while agitating the cell suspension on a vortex. Cells were then fixed for at least 2
328 hours at -20°C before proceeding with 3 washing steps in PBS, alternated by centrifugation (700 g, 5
329 min) with no brake. Afterwards, cell pellet was resuspended in 100 µL of DNAse-free RNAseA (0.5
330 µg/mL; Life Tech, 12091021) and incubated for 10 min at 37 °C. Cells were incubated with 100 µL
331 of propidium iodide (50 µg/mL) for 30 minutes, at room temperature, before proceeding to the
332 analysis. For cell cycle analysis, organoids were treated with 10 µM EdU for 3 hours. Afterwards,
333 organoids were harvested, dissociated into single cells, and filtered through a 30 µm strainer. Cells
334 were pelleted and stained with the Click-iT™ Plus EdU Alexa Fluor™ 488 Flow Cytometry Assay
335 Kit (Thermo Fisher Scientific, C10632), according to the manufacturer protocol. After the
336 incorporation of the fluorescent probe, cells were incubated with TO-PRO™-3 Iodide (Life Tech,
337 T3695) to stain for DNA content, before proceeding to the analysis. Flow cytometry was performed
338 with a FACS Canto (BD) analyser, and data analysed with Flow Jo v.10.
339 **Histology, immunostaining, and live imaging.**
340 Organoids were cultured for 5-7 days, released from the basement membrane as described above,
341 seeded in a neutralized collagen type-I solution (Corning, 354249), and cultured for additional 24
342 hours, before proceeding to fixation in 4% paraformaldehyde (Sigma Aldrich, P6148) for 5 hours, at
343 room temperature. Prostate tissue was harvested and immediately fixed using the same conditions.
344 Paraffin embedding and 5 µm sectioning were carried out according to standard procedures. For

345 immunofluorescence studies, antigen retrieval was performed using a citrate-based buffer (pH 6.0)
346 (Vector Lab, H3300). Slides were incubated in blocking solution (5% FBS + 0.1% Triton-X in PBS),
347 before proceeding to staining with primary antibodies, at 4°C, overnight. After three washes,
348 spectrally distinct fluorochrome-conjugated antibodies were incubated for 2 hours at room
349 temperature. After three additional washes, samples were counterstained with Hoechst 33342
350 (Abcam, ab145597), and the coverslip was applied, using FluorSave mounting medium (Merck,
351 345789). For immunohistochemistry studies, a similar protocol was followed, but using biotin-
352 conjugated secondary antibodies. The detection was performed using the Vectastain® Elite ABC
353 Peroxidase kit (Vector Labs, PK-6100) according to the manufacturer instructions. The final reaction
354 was blocked by washing slides with water, and coverslips were applied using the DPX mounting
355 medium (Sigma, 06522). For haematoxylin and eosin (H&E) staining, deparaffinised sections were
356 incubated with Gill haematoxylin (Merck, GH5232) for 2 minutes and washed with water. Samples
357 were washed with ethanol, incubated with eosin Y (Merck, HT110132) for 3 minutes, washed again
358 twice with ethanol, and treated with xylene, before mounting the coverslips in phenol based mounting
359 medium. For immunostaining with anti-Egfr and anti-Acvr1b antibodies, the urogenital apparatus
360 was isolated, snap-frozen in 2-methyl-buthanol cooled in liquid nitrogen, and cryo-sectioned at 20
361 µm. Tissue slides were fixed in 4% paraformaldehyde for 20 minutes at room temperature, before
362 proceeding as described above. For live imaging, organoids were stably transduced with pLenti-AIB-
363 EGFP. Images were acquired using either a Zeiss Axio Imager M2, or a Zeiss Axio Observer Z1
364 Apotome, or a Leica TCS SP8 Confocal. Image analysis was performed with the Zeiss ZEN software
365 or ImageJ (v.2.0.0-rc-69/1.52i)[65]. Primary antibodies are listed in Supplementary Table 2.

366 **RNA extraction.**

367 Total RNA was extracted using the RNeasy Plus Micro kit (Qiagen, 74034) according to the
368 manufacturer instructions, and analysed with an Agilent BioAnalyzer 2100 to confirm integrity (RIN
369 > 8), before proceeding with downstream applications.

370 **End-point semi-quantitative and quantitative real-time PCR.**

371 RNA was retrotranscribed into cDNA using the iScript™ cDNA synthesis kit (BioRad, 1708891).
372 End-point PCR was performed using Phusion Universal qPCR Kit (Life Tech, F566L), with PCR
373 products visualized by standard gel electrophoresis. For quantitative real-time gene expression
374 analysis, the qPCRBIO SyGreen Mix (PCRBiosystems, PB20.14-05) was used according to the
375 manufacturer instructions. At least three independent biological replicates were run for each sample,
376 using the CFX96 Real Time PCR thermocycler (Bio-Rad). The data were processed using Bio-Rad
377 CFX Manager software (v.3.1), while gene expression quantification and statistical analyses were

378 performed with GraphPad PRISM (v.6.01). Primer sequences are included in Supplementary Table
379 3.

380 **RNA sequencing and data analysis.**

381 cDNA libraries were prepared with TruSeq stranded mRNA library prep Kit (Illumina, RS-122-2101)
382 using 1 µg of total RNA. RNA sequencing was performed on an Illumina HiSeq 2500 Sequencer
383 using standard Rapid Run conditions at the Next-Generation Sequence Facility of University of
384 Trento. The obtained reads were 100 bp long, single ends, and 25 million on average for each sample.
385 FASTQ file from Illumina HiSeq2500 sequencing machine underwent adapter removal and quality-
386 base trimming using Trimmomatic-v0.35. Genomic alignments were performed onto the Mouse
387 genome (mm10 assembly version) using STAR-v2.6.0 aligner with a maximum mismatch of two and
388 default settings for all other parameters. Then, uniquely mapped reads were selected and processed
389 with HTSeq-count v0.5.4 tool to obtain gene-level raw counts based on GRCm38.92 Ensembl
390 (www.ensembl.org) annotation. Genes with CPM (Counts Per Million) < 1 in all replicates were
391 considered unexpressed and hence removed from the analysis. TMM (Trimmed Mean of M values)
392 normalization and CPM conversion were next performed to obtain gene expression levels for
393 downstream analyses. For each comparison, differential expression testing was performed using the
394 edgeR-3.20.9 statistical package. According to the edgeR workflow, both common (all genes in all
395 samples) and separate (gene-wise) dispersions were estimated and integrated into a Negative
396 Binomial generalized linear model to moderate gene variability across samples. For each comparison,
397 genes having a log Fold-change outside the range of +/-1.5 and a FDR q-value equal or smaller than
398 0.01 were considered as differentially expressed between the two groups.

399 **Gene Set Enrichment Analysis (GSEA).**

400 For the gene set enrichment analysis, the GSEA software (v4.0.3) was run in the 'pre-ranked' mode
401 using the Fold-change as a ranking metric and an FDR enrichment threshold of 0.25. Gene sets were
402 directly obtained from the Molecular Signature (MSig) database (http://
403 software.broadinstitute.org/gsea/msigdb) focusing on all available sets reported in the following
404 MSigDB collections: C2 (curated gene sets): Biocarta, Kegg, Reactome; C5 (Gene ontology):
405 Biological Processes, Cellular Component, Molecular Function; C6 (oncogenic signatures) and C7
406 (immunologic signatures).

407 **Principal Component Analysis (PCA).**

408 PCA was performed using the DESeq2 R-package[66] as follows: normalized counts (CPM) were firstly
409 converted into a DESeqDataset object through a DESeqDatasetFromMatrix function with default
410 parameters and transformed through the variantStabilizingTransformation function to stabilize

411 variance-mean relation across samples. Then, transformed data was analyzed by PCA (plotPCA
412 function) generating a two-dimensional space where the two first components are represented.

413 **Subcellular Fractionation and Western blotting.**

414 Cell pellets from organoid cultures were obtained as previously described and lysed in fresh RIPA
415 buffer (50 mM Tris-HCl, pH 7.5, 150 mM NaCl, 1% Triton X-100, 1% sodium deoxycholate, 1%
416 NP-40) supplemented with protease (Halt™ protease inhibitor cocktail, Life Tech, 87786) and
417 phosphatase inhibitors (Phosphatase-Inhibitor Mix II solution, Serva, 3905501). Nuclear/cytoplasmic
418 fractionation was performed using NE-PER Nuclear and Cytoplasmic Extraction Kit (Life Tech,
419 78833) according to the manufacturer instructions. Protein concentrations were measured using the
420 BCA Protein Assay Kit (Pierce™ BCA Protein Assay kit, Thermo Fisher Scientific, 23225) and a
421 Tecan Infinite M200 Plate Reader.

422 Protein extracts were resolved via SDS-PAGE, transferred to polyvinylidene difluoride (PVDF)
423 membrane (Merck, GE10600023) using a wet electroblotting system (Bio-Rad). The membranes
424 were blocked with 5% non-fat dry milk or 5% BSA in TBS-T (50 mM Tris-HCl, pH 7.5, 150 mM
425 NaCl, 0.1% Tween20) for 1 hour, at room temperature, and then incubated with gentle shaking with
426 designated primary antibodies overnight, at 4°C. Membranes were incubated with HRP-conjugated
427 secondary antibody in blocking buffer for 1 hour at room temperature. Immunoreactive bands were
428 detected using ECL LiteAblot plus kit A+B (Euroclone, GEHRPN2235) with an Alliance LD2 device
429 and software (UVITEC). Primary antibodies are provided in Supplementary Table 4.

430 **Click-it chemistry-based mass spectrometry analysis.**

431 Organoids were seeded at the approximate concentration of 50,000 cells/ml, depositing seven 40 ul
432 domes *per* individual well of a 6-well non-tissue culture plate. Three wells were used for each
433 condition. Following methionine depletion (2 hours), organoids were grown overnight at 37 °C with
434 L-azidohomoalanine (AHA) medium. Conditioned supernatants were collected, supplemented with
435 protease inhibitors, and stored at -80 °C until further processing. CLICK-IT enrichment of AHA-
436 labelled secreted proteins was performed with the Click-iT™ protein enrichment kit (Thermo Fisher
437 Scientific, C10416) as previously described[67,68]. Following trypsin digestion, peptides were purified
438 by reversed-phase (C18) stage-tip purification[69]. LC-MS/MS analysis was performed by an EASY-
439 LC 1000 coupled to a Q-Exactive mass spectrometer (Thermo Fisher Scientific). LC-MS/MS data
440 analysis was conducted using the MaxQuant/Perseus software suite.

441 **Enzyme-linked immunosorbent assay (ELISA).**

442 Activin A quantification was performed using the corresponding Quantikine ELISA Kit (R&D
443 Systems, DAC00B) according to the manufacturer instructions.
444 **Karyotype analysis.**
445 Organoid cultures were treated with nocodazole (15 μM; Sigma, SML1665) for 5 hours. Organoids
446 were recovered from basement membrane, and 900 μL/sample of 50 mM KCl were added to the cell
447 pellet dropwise, followed by 10 minutes of incubation at 37 °C. After centrifugation (200 g, 5
448 minutes) 900 μL/sample of Carnoy's fixative (methanol/acetic acid 3:1) was added dropwise.
449 Samples were resuspended and incubated for 10 minutes at 37 °C, followed by three washes with
450 methanol/acetic acid 2:1. Approximately 25,000 cells/samples were resuspended in 50 μL and
451 dropped from at least 1 meter of height, directly on a glass slide. After air-drying, the glass slide was
452 incubated with Hoechst 33342, at room temperature, for 10 minutes, and then washed with
453 methanol/acetic acid 2:1 for 5 minutes. After air-drying, coverslips were mounted with ProLong Gold
454 Antifade (Invitrogen, P36934). Images were acquired at the Zeiss Observer Z1 microscope and
455 analysed with ImageJ (v2.0.0-rc-69/1.52i)[65].
456 **Multicolor FISH (M-FISH), Chromosome painting and Telomeric FISH.**
457 For M-FISH, fixed cells were dropped onto glass slides and hybridized with the 21XMouse
458 Multicolor FISH Probe Kit (MetaSystems, D-0425-060-DI), as previously described[70]. Briefly, the
459 slides were denatured in 0.07 N NaOH and then rinsed in a graded ethanol series. The probe mix was
460 denatured using a MJ mini personal thermal cycler (Bio-Rad) with the following program: 5 minutes
461 at 75 °C, 30 seconds at 10 °C, and 30 minutes at 37 °C. The probe was added to the slides and the
462 coverslip was sealed using rubber cement. The samples were then hybridized in a humidified chamber
463 at 37 °C for 48 h, washed in saline-sodium citrate (SSC) buffer for 5 min at 75 °C, and finally
464 counterstained with DAPI (Abcam, 6843.2), in Vectashield mounting medium. Metaphases were
465 visualized and captured using a Zeiss Axio-Imager M1 microscope. The karyotyping and cytogenetic
466 analysis of each single chromosome was performed using the M-FISH module of the ISIS software
467 (MetaSystems). A total of 25 metaphases for each sample spreads were analysed in two independent
468 experiments.
469 For chromosome painting, fixed cells were dropped onto glass slides and hybridized with
470 enumeration XMP painting probes specific for chromosomes X (red label) and chromosome Y (green
471 label) (MetaSystems, D-1420-050-OR, D-1421-050-FI) following the manufacturer instructions.
472 Briefly, probes were applied to the slides, denatured at 75 °C for 2 minutes, and then incubated at 37
473 °C overnight. The slides were washed in SSC and counterstained with DAPI in antifade reagent
474 (MetaSystems, D-0902-500-DA). Metaphases were visualized and captured using a Zeiss Axio-

475 Imager M1 microscope. A total of 100 metaphases were analysed for each sample in two independent
476 experiments.
477 For telomeric FISH, staining was performed as previously described[71]. Briefly, slides and the Cy3
478 linked telomeric (TTAGGG)3 PNA probe, (DAKO Cytomatation, K5326) were co-denatured at 80
479 °C for 3 minutes, and hybridized for 2 hours at room temperature, in a humidified chamber. After
480 hybridization, slides were washed and then dehydrated with an ethanol series and air dried. Finally,
481 slides were counterstained with DAPI and Vectashield. Images were captured at 63× magnification
482 using a Zeiss Axio-Imager M1 microscope, and the telomere signals were analysed using the ISIS
483 software (MetaSystems). Telomere doublets frequency was calculated as the ratio between the
484 number of doublets signals and the total number of chromosomes in each metaphase analysed[72]. At
485 least 20 metaphases in two independent experiments were analysed.
486 **Orthotopic organoid transplantation.**
487 Orthotopic transplantation of organoids into the prostate of syngeneic immune-competent C57BL/6J
488 mice was performed adapting a previously published method[73]. Organoids were dissociated as
489 described above, with 50,000 cells *per* injection resuspended in 10 μL of 50% basement matrix,
490 supplemented with methylene blue (as tracer). Upon abdominal incision of the host, the left anterior
491 prostate lobe was exposed, and injected into the distal part. The contralateral lobe was injected with
492 saline as negative control. Mice were regularly monitored and sacrificed after 6 months for tissue
493 collection and histopathological analysis.
494 **Statistical analysis and reproducibility.**
495 No statistical methods were used to predetermine sample size. The *in vitro* experiments were not
496 randomized, and the investigators were not blinded to allocation during experiments and outcome
497 assessment. The *in vivo* transplantation experiments were randomized, and the investigators were
498 blinded to allocation during experiments and outcome assessment. The *in vitro* experiments were
499 carried out on organoid lines derived from at least two distinct animals and repeated at least three
500 independent times. The *in vivo* transplantation experiments were based on two distinct organoid lines
501 and were repeated at least two independent times. Data collection was performed using Microsoft
502 Office Excel 2016–2018 and statistical analysis was performed using GraphPad Prism 6 software.
503 The number of replicates, the format of the data, and the statistical tests are indicated in figure legends.
504 p-values < 0.05 were considered significant.

505 ## Data availability

506 RNA sequencing datasets have been deposited on BioProject with the dataset identifier
507 PRJNA659468. All other data supporting the findings of this study are available from the
508 corresponding authors upon reasonable request.

509 **References**

510 1. De Marzo, A. M., Nelson, W. G., Meeker, A. K. & Coffey, D. S. Stem cell features of benign
511 and malignant prostate epithelial cells. *The Journal of urology* **160**, 2381–92 (1998).
512 2. Toivanen, R. & Shen, M. M. Prostate organogenesis: tissue induction, hormonal regulation and
513 cell type specification. *Development* **144**, 1382–1398 (2017).
514 3. Ørsted, D. D. & Bojesen, S. E. The link between benign prostatic hyperplasia and prostate
515 cancer. *Nature Reviews Urology* **10**, 49–54 (2013).
516 4. Shinohara, D. B. *et al.* A mouse model of chronic prostatic inflammation using a human
517 prostate cancer-derived isolate of Propionibacterium acnes. *The Prostate* **73**, 1007–1015 (2013).
518 5. Kwon, O.-J., Zhang, L., Ittmann, M. M. & Xin, L. Prostatic inflammation enhances basal-to-
519 luminal differentiation and accelerates initiation of prostate cancer with a basal cell origin.
520 *Proceedings of the National Academy of Sciences of the United States of America* **111**, E592-
521 600 (2014).
522 6. Simons, B. W. *et al.* A human prostatic bacterial isolate alters the prostatic microenvironment
523 and accelerates prostate cancer progression. *The Journal of Pathology* **235**, 478–489 (2015).
524 7. Kirby, R. S., Lowe, D., Bultitude, M. I. & Shuttleworth, K. E. D. Intra-prostatic Urinary Reflux:
525 an Aetiological Factor in Abacterial Prostatitis. *British Journal of Urology* **54**, 729–731 (1982).
526 8. DuPre, N. C. *et al.* Corpora amylacea in prostatectomy tissue and associations with molecular,
527 histological, and lifestyle factors. *The Prostate* **78**, 1172–1180 (2018).
528 9. Nakai, Y., Nelson, W. G. & Marzo, A. M. D. The Dietary Charred Meat Carcinogen 2-Amino-
529 1-Methyl-6-Phenylimidazo[4,5-b]Pyridine Acts as Both a Tumor Initiator and Promoter in the
530 Rat Ventral Prostate. *Cancer Res* **67**, 1378–1384 (2007).
531 10. Kwon, O.-J., Zhang, B., Zhang, L. & Xin, L. High fat diet promotes prostatic basal-to-luminal
532 differentiation and accelerates initiation of prostate epithelial hyperplasia originated from basal
533 cells. *Stem Cell Research* **16**, 682–691 (2016).
534 11. Zhang, B. *et al.* Non-Cell-Autonomous Regulation of Prostate Epithelial Homeostasis by
535 Androgen Receptor. *Molecular Cell* **63**, 976–989 (2016).
536 12. Wang, Z. *et al.* Androgenic to oestrogenic switch in the human adult prostate gland is regulated
537 by epigenetic silencing of steroid 5α-reductase 2. *The Journal of Pathology* **243**, 457–467
538 (2017).
539 13. Crowell, P. D. *et al.* Expansion of Luminal Progenitor Cells in the Aging Mouse and Human
540 Prostate. *Cell Reports* **28**, 1499-1510.e6 (2019).
541 14. Sfanos, K. S., Yegnasubramanian, S., Nelson, W. G. & De Marzo, A. M. The inflammatory
542 microenvironment and microbiome in prostate cancer development. *Nature Reviews Urology*
543 **15**, 11–24 (2018).
544 15. de Bono, J. S. *et al.* Prostate carcinogenesis: inflammatory storms. *Nature Reviews Cancer* **20**,
545 455–469 (2020).

546 16. Tucker, R. F., Shipley, G. D., Moses, H. L. & Holley, R. W. Growth inhibitor from BSC-1 cells
547 closely related to platelet type beta transforming growth factor. *Science* **226**, 705–707 (1984).
548 17. Moses, H. L., Roberts, A. B. & Derynck, R. The Discovery and Early Days of TGF-β: A
549 Historical Perspective. *Cold Spring Harb Perspect Biol* **8**, a021865 (2016).
550 18. Mc Keehan, W. L. & Adams, P. S. Heparin-binding growth factor/prostatropin attenuates
551 inhibition of rat prostate tumor epithelial cell growth by transforming growth factor type beta.
552 *In Vitro Cell Dev Biol* **24**, 243–246 (1988).
553 19. Massagué, J. TGFβ signalling in context. *Nature Reviews Molecular Cell Biology* **13**, 616–630
554 (2012).
555 20. Derynck, R. & Budi, E. H. Specificity, versatility, and control of TGF-β family signaling. *Sci.*
556 *Signal.* **12**, eaav5183 (2019).
557 21. Bailey, P. *et al.* Genomic analyses identify molecular subtypes of pancreatic cancer. *Nature*
558 **531**, 47–52 (2016).
559 22. Yaeger, R. *et al.* Clinical Sequencing Defines the Genomic Landscape of Metastatic Colorectal
560 Cancer. *Cancer Cell* **33**, 125-136.e3 (2018).
561 23. David, C. J. & Massagué, J. Contextual determinants of TGFβ action in development, immunity
562 and cancer. *Nature Reviews Molecular Cell Biology* **19**, 419–435 (2018).
563 24. Gerstung, M. *et al.* The evolutionary history of 2,658 cancers. *Nature* **578**, 122–128 (2020).
564 25. Salm, S. N. *et al.* TGF-β maintains dormancy of prostatic stem cells in the proximal region of
565 ducts. *J Cell Biol* **170**, 81–90 (2005).
566 26. Wei, X. *et al.* Spatially Restricted Stromal Wnt Signaling Restrains Prostate Epithelial
567 Progenitor Growth through Direct and Indirect Mechanisms. *Cell Stem Cell* **2,** 24(5):753-
568 768.e6. (2019).
569 27. Henry, G. H. *et al.* A Cellular Anatomy of the Normal Adult Human Prostate and Prostatic
570 Urethra. *Cell Reports* **25**, 3530-3542.e5 (2018).
571 28. Karthaus, W. R. *et al.* Regenerative potential of prostate luminal cells revealed by single-cell
572 analysis. *Science* **368**, 497–505 (2020).
573 29. Joseph, D. B. *et al.* Urethral luminal epithelia are castration-insensitive cells of the proximal
574 prostate. *The Prostate* **80**, 872–884 (2020).
575 30. Guo, W. *et al.* Single-cell transcriptomics identifies a distinct luminal progenitor cell type in
576 distal prostate invagination tips. *Nature Genetics* **52**, 908–918 (2020).
577 31. Crowley, L. *et al.* A single-cell atlas of the mouse and human prostate reveals heterogeneity and
578 conservation of epithelial progenitors. *eLife* **9**, e59465 (2020).
579 32. Mevel, R. *et al.* RUNX1 marks a luminal castration resistant lineage established at the onset of
580 prostate development. *eLife* **9**, e60225 (2020).
581 33. Pignon, J.-C. *et al.* Cell Kinetic Studies Fail to Identify Sequentially Proliferating Progenitors as
582 the Major Source of Epithelial Renewal in the Adult Murine Prostate. *PLOS ONE* **10**, e0128489
583 (2015).
584 34. Kwon, O.-J. *et al.* The Sca-1+ and Sca-1− mouse prostatic luminal cell lineages are
585 independently sustained. *Stem Cells* **38,** 1479-1491 (2020).
586 35. Kwon, O.-J., Zhang, L. & Xin, L. Stem Cell Antigen-1 Identifies a Distinct Androgen-
587 Independent Murine Prostatic Luminal Cell Lineage with Bipotent Potential. *Stem Cells* **34**,
588 191–202 (2016).

589 36. Karthaus, W. R. *et al.* Identification of multipotent luminal progenitor cells in human prostate
590 organoid cultures. *Cell* **159**, 163–175 (2014).
591 37. Chua, C. W. *et al.* Single luminal epithelial progenitors can generate prostate organoids in
592 culture. *Nature Cell Biology* **16**, 951–961 (2014).
593 38. Barros-Silva, J. D. *et al.* Single-Cell Analysis Identifies LY6D as a Marker Linking Castration-
594 Resistant Prostate Luminal Cells to Prostate Progenitors and Cancer. *Cell Reports* **25**, 3504-
595 3518.e6 (2018).
596 39. Sporn, M. B. & Todaro, G. J. Autocrine Secretion and Malignant Transformation of Cells. *N*
597 *Engl J Med* **303**, 878-80 (1980)
598 40. Eichelbaum, K., Winter, M., Diaz, M. B., Herzig, S. & Krijgsveld, J. Selective enrichment of
599 newly synthesized proteins for quantitative secretome analysis. *Nature Biotechnology* **30**, 984–
600 990 (2012).
601 41. Nakamura, T. *et al.* Activin-binding protein from rat ovary is follistatin. *Science* **247**, 836–838
602 (1990).
603 42. Yamaguchi, K. *et al.* Identification of a Member of the MAPKKK Family as a Potential
604 Mediator of TGF-β Signal Transduction. *Science* **270**, 2008–2011 (1995).
605 43. Shim, J.-H. *et al.* TAK1, but not TAB1 or TAB2, plays an essential role in multiple signaling
606 pathways in vivo. *Genes Dev.* **19**, 2668–2681 (2005).
607 44. Sato, S. *et al.* Essential function for the kinase TAK1 in innate and adaptive immune responses.
608 *Nature Immunology* **6**, 1087–1095 (2005).
609 45. Sorrentino, A. *et al.* The type I TGF-β receptor engages TRAF6 to activate TAK1 in a receptor
610 kinase-independent manner. *Nature Cell Biology* **10**, 1199–1207 (2008).
611 46. Platanias, L. C. Mechanisms of type-I- and type-II-interferon-mediated signalling. *Nature*
612 *Reviews Immunology* **5**, 375–386 (2005).
613 47. Kretzschmar, K. & Clevers, H. Organoids: Modeling Development and the Stem Cell Niche in
614 a Dish. *Developmental Cell* **38**, 590–600 (2016).
615 48. Huch, M., Knoblich, J. A., Lutolf, M. P. & Martinez-Arias, A. The hope and the hype of
616 organoid research. *Development* **144**, 938–941 (2017).
617 49. Cancilla, B. *et al.* Regulation of Prostate Branching Morphogenesis by Activin A and
618 Follistatin. *Developmental Biology* **237**, 145–158 (2001).
619 50. Gold, E. & Risbridger, G. Activins and activin antagonists in the prostate and prostate cancer.
620 *Molecular and Cellular Endocrinology* **359**, 107–112 (2012).
621 51. Ding, Z. *et al.* SMAD4-dependent barrier constrains prostate cancer growth and metastatic
622 progression. *Nature* **470**, 269–273 (2011).
623 52. Gerke, T. A. *et al.* Evaluating a 4-marker signature of aggressive prostate cancer using time-
624 dependent AUC. *The Prostate* **75**, 1926–1933 (2015).
625 53. Lu, X. *et al.* Opposing roles of TGFβ and BMP signaling in prostate cancer development.
626 *Genes & Development* **31**, 2337–2342 (2017).
627 54. Abeshouse, A. *et al.* The Molecular Taxonomy of Primary Prostate Cancer. *Cell* **163**, 1011–
628 1025 (2015).
629 55. Li, J. *et al.* A genomic and epigenomic atlas of prostate cancer in Asian populations. *Nature*
630 **580**, 93–99 (2020).

631 56. Washino, S. *et al.* Loss of MAP3K7 Sensitizes Prostate Cancer Cells to CDK1/2 Inhibition and
632 DNA Damage by Disrupting Homologous Recombination. *Mol Cancer Res* **17**, 1985–1998
633 (2019).
634 57. Paull, E. O. *et al.* A modular master regulator landscape controls cancer transcriptional identity.
635 *Cell* **184**, 334-351.e20. (2021).
636 58. He, M. X. *et al.* Transcriptional mediators of treatment resistance in lethal prostate cancer.
637 *Nature Medicine* 1-8 (2021).
638 59. Krausgruber, T. *et al.* Structural cells are key regulators of organ-specific immune responses.
639 *Nature* **583**, 296–302 (2020).
640 60. Vergote, I. *et al.* A randomized, double-blind, placebo-controlled phase 1b/2 study of
641 ralimetinib, a p38 MAPK inhibitor, plus gemcitabine and carboplatin versus gemcitabine and
642 carboplatin for women with recurrent platinum-sensitive ovarian cancer. *Gynecologic Oncology*
643 **156**, 23–31 (2020).
644 61. Oshimori, N., Oristian, D. & Fuchs, E. TGF-β Promotes Heterogeneity and Drug Resistance in
645 Squamous Cell Carcinoma. *Cell* **160**, 963–976 (2015).
646 62. Quinn, D. I., Sandler, H. M., Horvath, L. G., Goldkorn, A. & Eastham, J. A. The evolution of
647 chemotherapy for the treatment of prostate cancer. *Annals of Oncology* **28**, 2658–2669 (2017).
648 63. Akhurst, R. J. & Hata, A. Targeting the TGFβ signalling pathway in disease. *Nature Reviews*
649 *Drug Discovery* **11**, 790–811 (2012).
650 64. Drost, J. *et al.* Organoid culture systems for prostate epithelial and cancer tissue. *Nature*
651 *Protocols* **11**, 347–358 (2016).
652 65. Rueden, C. T. *et al.* ImageJ2: ImageJ for the next generation of scientific image data. *BMC*
653 *Bioinformatics* **18**, 529 (2017).
654 66. Love, M. I., Huber, W. & Anders, S. Moderated estimation of fold change and dispersion for
655 RNA-seq data with DESeq2. *Genome Biology* **15**, 550 (2014).
656 67. Eichelbaum, K., Winter, M., Diaz, M. B., Herzig, S. & Krijgsveld, J. Selective enrichment of
657 newly synthesized proteins for quantitative secretome analysis. *Nature Biotechnology* **30**, 984–
658 990 (2012).
659 68. Eihelbaum, K. & Krijgsveld, J. Combining Pulsed SILAC labeling and Click-Chemistry for
660 Quantitative Secretome Analysis. *Methods in Molecular Biology* **1174**, 101-114 (2014).
661 69. Rappsilber, J., Mann, M. & Ishihama, Y. Protocol for micro-purification, enrichment, pre-
662 fractionation and storage of peptides for proteomics using StageTips. *Nature Protocols* **2**, 1896–
663 1906 (2007).
664 70. Nieri, D. *et al.* Cyogenetics effects in AG01522 human primary fibroblasts exposed to low
665 doses of radiations with different quality. *International Journal of Radiation Biology* **89**, 698–
666 707 (2013).
667 71. Samper, E., Goytisolo, F. A., Slijepcevic, P., van Buul, P. P. W. & Blasco, M. A. Mammalian
668 Ku86 protein prevents telomeric fusions independently of the length of TTAGGG repeats and
669 the G-strand overhang. *EMBO reports* **1**, 244–252 (2000).
670 72. Berardinelli, F. *et al.* G-quadruplex ligand RHPS4 radiosensitizes glioblastoma xenograft in
671 vivo through a differential targeting of bulky differentiated- and stem-cancer cells. *Journal of*
672 *Experimental & Clinical Cancer Research* **38**, 311 (2019).
673 73. O'Rourke, K. P. *et al.* Transplantation of engineered organoids enables rapid generation of
674 metastatic mouse models of colorectal cancer. *Nature Biotechnology* **35**, 577–582 (2017).

Acknowledgments

We are grateful to Francesca Demichelis, Alberto Inga, Giannino del Sal, Marco Marcia, and Karuna Ganesh, for critical reading of the manuscript, and, Luciano Conti, Alessio Zippo, Luca Fava, Fulvio Chiacchiera, Luca Tiberi, Massimo Lopes, Alberto Briganti, Matteo Bellone and Marianna Kruithof-de Julio for fruitful discussions. We thank Francesca Demichelis, Massimo Pizzato, Luca Fava, Yari Ciribilli, and Valeria Poli, for sharing reagents. We thank Veronica de Sanctis, Roberto Bertorelli and Paola Fassan of the Next Generation Sequencing Facility of the University of Trento for RNA sequencing. We also thank Sergio Robbiati and Marta Tarter of the CIBIO Model Organism Facility, Marina Cardano of the CIBIO Cell Technology Facility, Giorgina Scarduelli and Michela Roccuzzo of the CIBIO Advanced Imaging Facility, Isabella Pesce of the CIBIO Cell Analysis and Separation Facility, Valentina Adami and Michael Pancher of the CIBIO High-Throughput Screening Facility, and Isabelle Bonomo for assistance with experiments. We are grateful to Qingwen Jiang and Ahmed Mahmoud for help with illustrations, which were created using Inkscape and Biorender.com. This study was primarily supported by grants from the Giovanni Armenise-Harvard Foundation (Career Development Award to A.L.), the Lega Italiana Lotta ai Tumori (LILT-Bolzano to A.L.), the Italian Ministry for Research and the University (MIUR PRIN 2017 to A.L.), the Associazione Italiana per la Ricerca sul Cancro (AIRC MFAG 2017-ID 206221 to A.R.), the NIH (R01CA238005 to M.M.S.) – and by core funding from the University of Trento. Individual fellowships were awarded from the United States Department of Defense (W81XWH-18-1-0424 to F.C.), the European Union (H2020-MSCA 749795 to A.Be.), the Fondazione Umberto Veronesi (FUV 2016 and 2017 to F.C., FUV 2016 to A.A., and FUV 2018 to A.Be.), and the University of Trento (Ph.D. fellowship to V.F, and D.D.F.).

Author contributions

F.C. made initial observations and designed the project in consultation with A.L.; F.C., V.F. and A.L. designed the experiments with the contribution of A.Ala. and D.D.F. regarding the Tak1/p38 MAPK signalling; F.C., with the contribution of M.Z., generated and characterized the normal prostate organoid lines described in this study; F.C., with the contribution of M.D.P., carried out the wet-lab based experiments defining the role of non-canonical Tgf-β signalling in the control of epithelial progenitor proliferation and the ability of progenitors to spontaneously evade such regulatory mechanism; F.C., V.F., E.B. and D.D.F. characterized the consequences of non-canonical Tgf-β signalling evasion in organoid cultures; V.F. generated the sh-Smad4 organoid line, with the contribution of D.D.F. and M.C., carried out the pharmacological studies on Tak1/p38 MAPK

706 signalling; V.F., A.Ala., and D.D.F. performed biochemical studies on cell cycle regulators and
707 mediators of the type-I interferon-like response; V.F., D.D.F, S.G., G.M. and A.L. performed
708 orthotopic transplantations; M.L. and M.G. executed Click-it mass spectrometry experiments and
709 analysed the data; A.Be. contributed to flow cytometry; S.G. executed immunostaining experiments
710 and contributed to image acquisition; A.Bi. contributed to the characterization of p53 function in
711 organoids; F.B. and A.Ant. carried out and analysed chromosome painting and FISH studies; M.B.,
712 M.F. and M.L provided histopathological annotations; F.G. and A.R. performed the computational
713 analyses; M.M.S. contributed to the interpretation of data; F.C. and V.F. assembled the figures; F.C.
714 wrote the first draft of the manuscript; F.C., V.F. and A.L. edited the manuscript with inputs from
715 F.B., A.Ant., A.R., M.L. and M.M.S.; A.L. acquired the main funding sources.

716 Competing interests

717 Authors declare no competing interests.

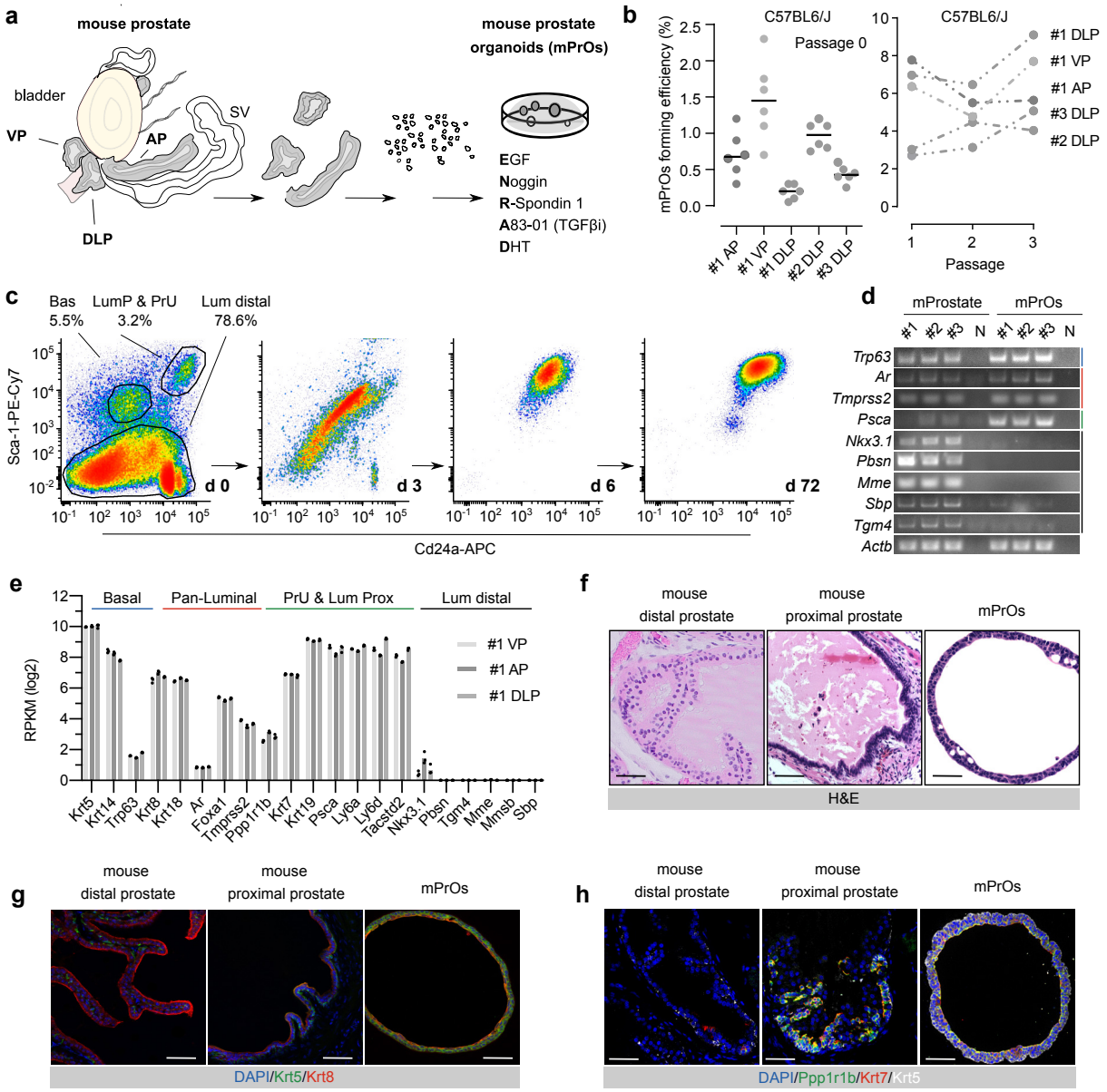

Mouse prostate organoids are highly enriched in epithelial progenitor cells

a. Schematic diagram describing organoid culture derivation (AP, Anterior Prostate; DLP, Dorso-Lateral Prostate; VP, Ventral Prostate; SV, Seminal Vesicle; DHT, dihydrotestosterone).
b. Mouse prostate organoid forming efficiency. Efficiency at derivation (left; data points are shown with crossing line representing mean value). Efficiency at passage 1-3 (right; n≥ 3 per organoid line/passage; data are presented as mean).
c. Representative longitudinal flow-cytometry analysis of dissociated organoid cells (Bas, Basal; LumP, Luminal Proximal; PrU, Periurethral; Lum Distal, Luminal Distal).
d. End-point RT-PCR analysis for selected marker genes.
e. Bulk-RNAseq analysis (n=3; individual data points are shown with bar graphs representing mean value).
f. Representative Haematoxylin-Eosin (H&E) staining of mouse prostate tissue and organoid sections (scale bars = 50 μm).
g. Representative Immunofluorescence (IF) analysis for selected markers in mouse prostate tissue and organoid sections (scale bars = 50 μm).
h. IF staining for selected markers in mouse prostate tissue and organoid sections (scale bars = 50 μm).

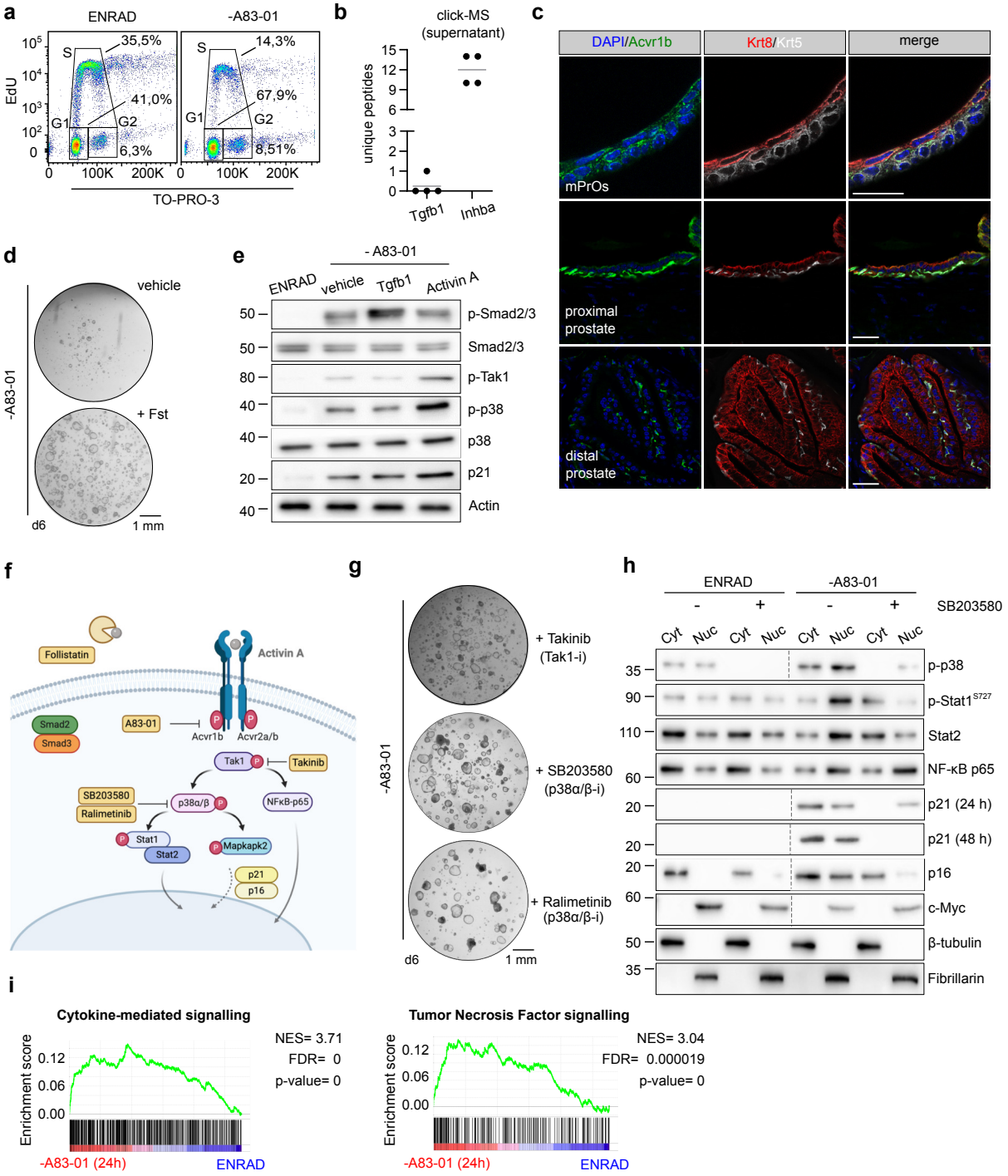

Intra-epithelial non-canonical Activin A signalling mediates the Tgf-β induced cytostatic response in mouse prostate organoids

a. Cell cycle analysis by flow cytometry (EdU *vs.* TO-PRO-3) in complete medium (ENRAD) or in the absence of A83-01 (24 hours).
b. Detection of proteins secreted by mouse prostate organoids in culture based on click-chemistry enrichment and mass spectrometry analysis (n=4; data points are shown with crossing line representing mean value).
c. IF analysis for selected markers in mouse prostate tissue and organoid sections (scale bar = 50 µm).
d. Representative stereoscopic images of mouse prostate organoids cultured in the absence of A83-01, with or without Follistatin (Fst, 500 ng/mL, 6 days).
e. Western blot (WB) analysis in mouse prostate organoids for selected canonical and non-canonical Tgf-β signalling mediators, and the cell cycle inhibitor p21 (Activin A, 50 ng/mL; Tgfb1, 500 ng/mL; 24 hours).
f. Schematic view of the non-canonical Activin A pathway, including inhibitors used for the experiments described in this figure.
g. Representative stereoscopic images of mouse prostate organoids following treatment with Takinib (Tak1 inhibitor; 5 µM, 6 days), SB203580 (p38α/β inhibitor; 10 µM, 6 days) or the structurally unrelated Ralimetinib (p38α/β inhibitor; 1 µM, 7 days).
h. Nuclear fractionation and WB analysis in mouse prostate organoids for selected signalling mediators and cell cycle regulators, in the presence or absence of SB203580 (p38α/β inhibitor; 10 µM, 24 hours).
i. Gene set enrichment analysis (GSEA) plots displaying significant enrichment for cytokine-mediated and Tumour Necrosis Factor (TNF) signalling in mouse prostate organoids cultured without A83-01 (24 hours) versus complete medium (ENRAD).

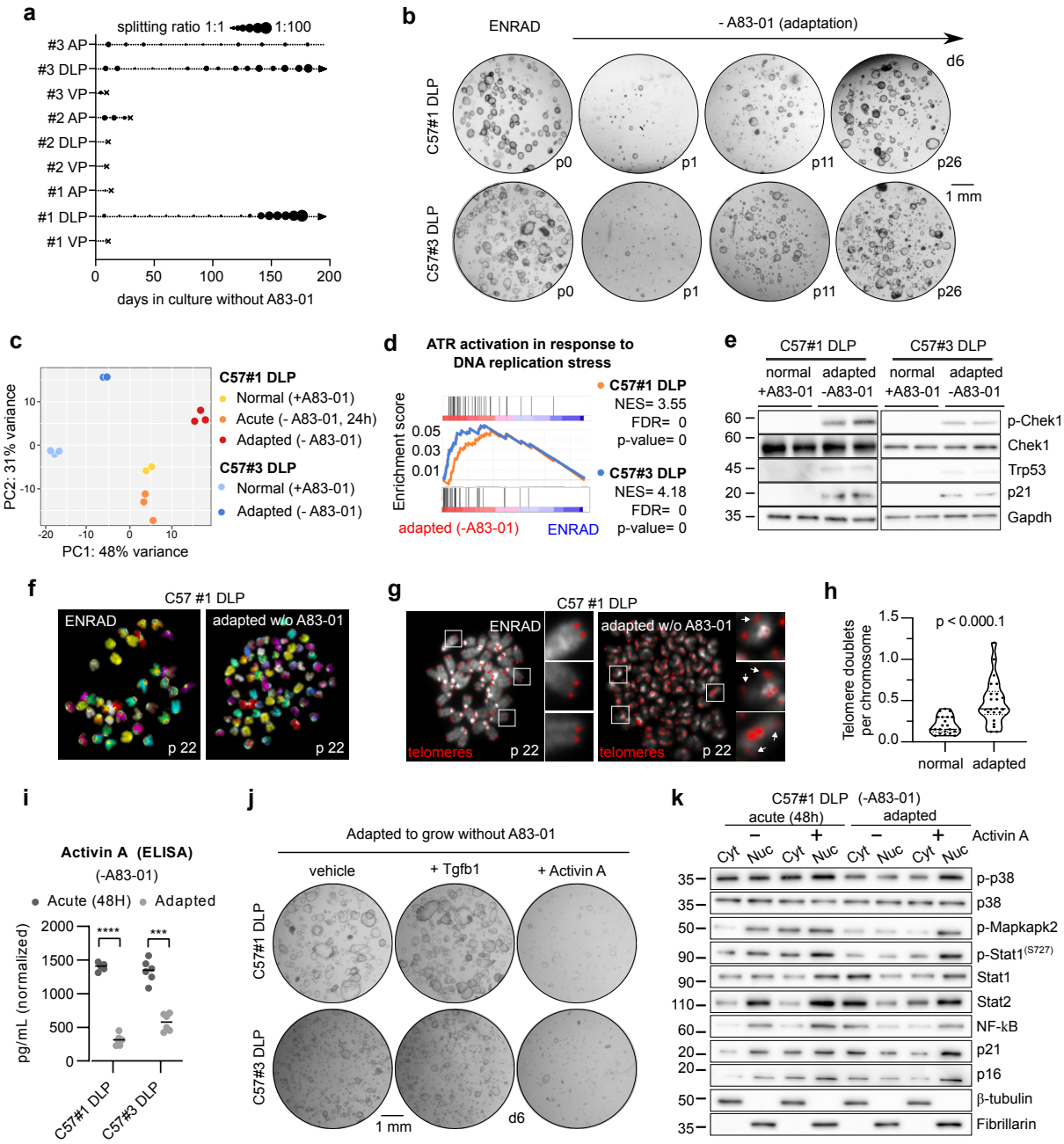

Evasion from the Tgf-β induced cytostatic response occurs via downregulation of intra-epithelial Activin A signalling and leads to DNA replication stress and genomic instability.

a. Diagram depicting the expansion of mouse prostate organoid cultures in the absence of the Tgf-β ligand inhibitor A83-01 (arrow = continuous expansion; dot = passage; cross = culture loss).

b. Representative stereoscopic images of C57BL/6J DLP #1 and # 3 mouse prostate organoid lines during adaptation in the absence of A83-01.

c. Principal Component Analysis (PCA) based on bulk RNA-sequencing of C57#1 DLP and C57#3 DLP mouse prostate organoids grown in normal conditions (ENRAD), upon acute A83-01 depletion (-A83-01, 24 hours) (C57#1 DLP only) or following adaptation (-A83-01, long-term).

d. Gene set enrichment analysis (GSEA) plot displaying significant enrichment for activation of ATR signalling in mouse prostate organoid lines (C57#1 DLP, top; C57#3 DLP, bottom) adapted to grow in the absence of A83-01 *vs.* normal control organoids cultured in complete medium (ENRAD).

e. WB analysis in C57#1 and C57# 3 DLP mouse prostate organoid lines adapted to grow in the absence of A83-01 *vs.* normal control organoids cultured in complete medium (ENRAD). Immunoblots are displayed for Chek1 (ATR signalling mediator), Trp53 and p21.

f. Representative spectral karyotype (SKY) images of metaphase spreads obtained from C57#1 DLP mouse prostate organoids cultured in normal conditions (ENRAD) or upon adaptation without A83-01. Widespread genomic instability is observed following adaptation.

g-h. Representative telomere FISH images - and quantification - in C57#1 DLP mouse prostate organoids cultured in normal conditions (ENRAD) or upon adaptation without A83-01. Widespread telomeric instability is observed following adaptation.

i. Enzyme-linked immunosorbent assay (ELISA) for Activin A expression in the supernatant of C57#1 and C57# 3 DLP mouse prostate organoid lines, upon acute A83-01 removal (48 hours) or long-term adaptation. Two-way ANOVA, Sidak's test, p-value *** (<0.001), **** (<0.0001).

j. Representative stereoscopic images of C57#1 and C57# 3 DLP mouse prostate organoid lines adapted to the absence of A83-01 and subsequently treated with either Tgfb1 (500 ng/mL, 6 days) or Activin A (50 ng/mL, 6 days).

k. WB analysis in the C57#1 DLP mouse prostate organoid line upon acute removal (24 hours) or long-term adaptation to A83-01 removal, in the presence or absence of Activin A (50 ng/mL, 24 hours).

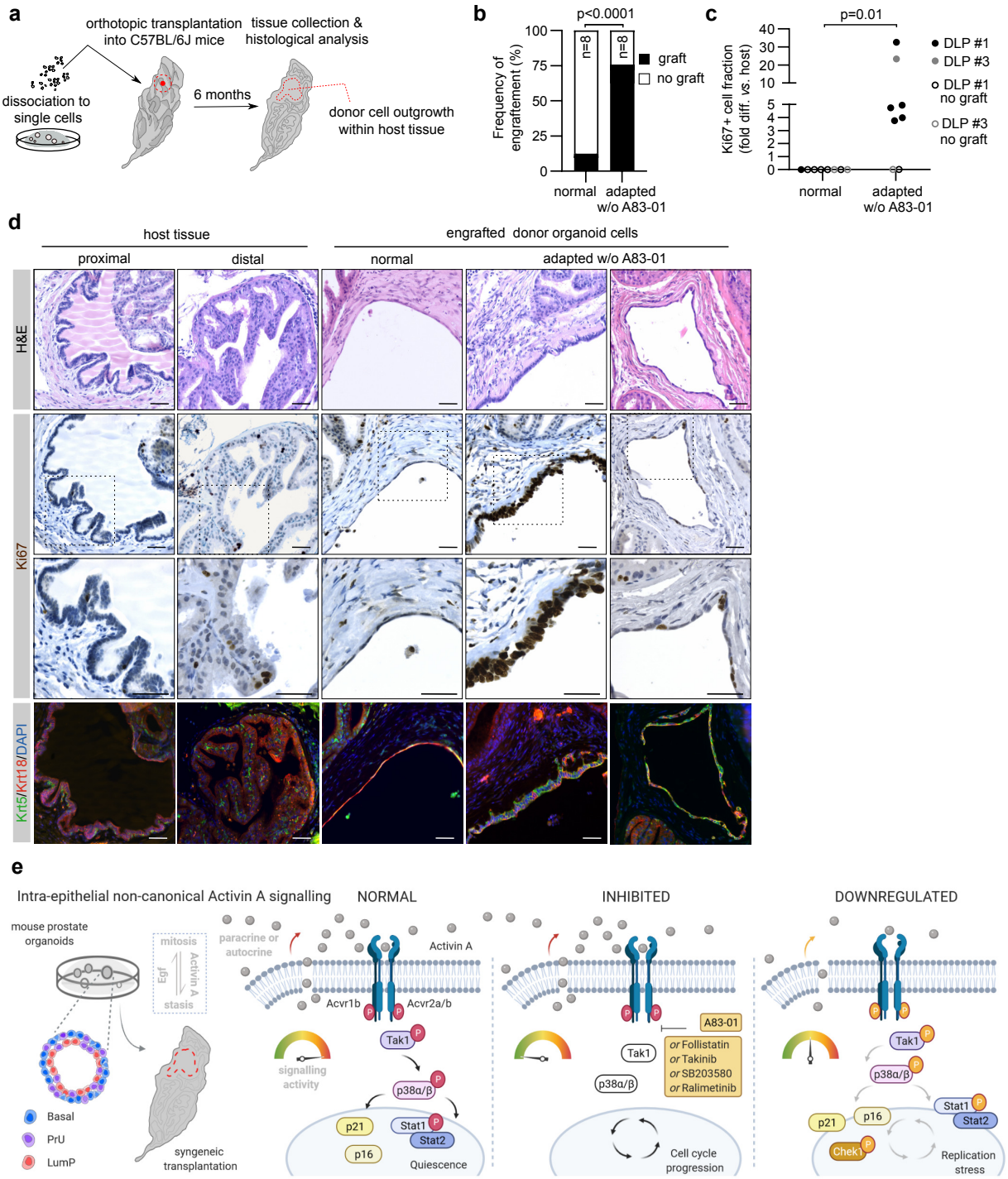

Enhanced engraftment of mouse prostate organoids with reduced Activin A signalling into immunocompetent hosts.

a. Schematic view of the orthotopic transplantation strategy into the anterior prostate lobe of immunocompetent syngeneic C57BL/6J mice.

b. Frequency of engraftment (%) of mouse prostate organoid lines (C57#1 DLP and C57#3 DLP) expanded in complete medium (normal) or adapted to the absence of A83-01 (binomial test (two-tailed)).

c. Normalized mitotic (Ki67+) cell index in grafts of mouse prostate organoid lines (C57#1 DLP and C57# 3 DLP) expanded in complete medium conditions (normal) or adapted to the absence of A83-01 (non-parametric Mann-Whitney test).

d. Representative H&E, IF, and immunohistochemistry (IHC) analyses of host prostate tissue and engrafted donor organoid cells (scale bar = 50 µm).

e. Intra-epithelial non-canonical Activin A signalling safeguards prostate progenitor quiescence. In normal circumstances, autocrine or paracrine Activin A triggers Tak1/p38 Mapk non-canonical signalling - antagonizing the pro-proliferative Egf pathway and enforcing cellular quiescence. Mechanistically, Tak1/p38 Mapk activity leads to p16 and p21 nuclear translocation - as well as to Stat1/2-dependent transcription of type-I interferon genes. Prostate organoid cultures require the suppression of this non-canonical signalling for continuous expansion, which can be achieved at different levels of the signalling cascade, using multiple inhibitors. Organoids with reduced levels on intra-epithelial Activin A signalling can be selected *in vitro*, and display enhanced engraftment efficiency *in vivo*, upon orthotopic transplantation into syngeneic hosts. Notably, the partial down-regulation of this pathway is associated with DNA replication stress and genomic instability.

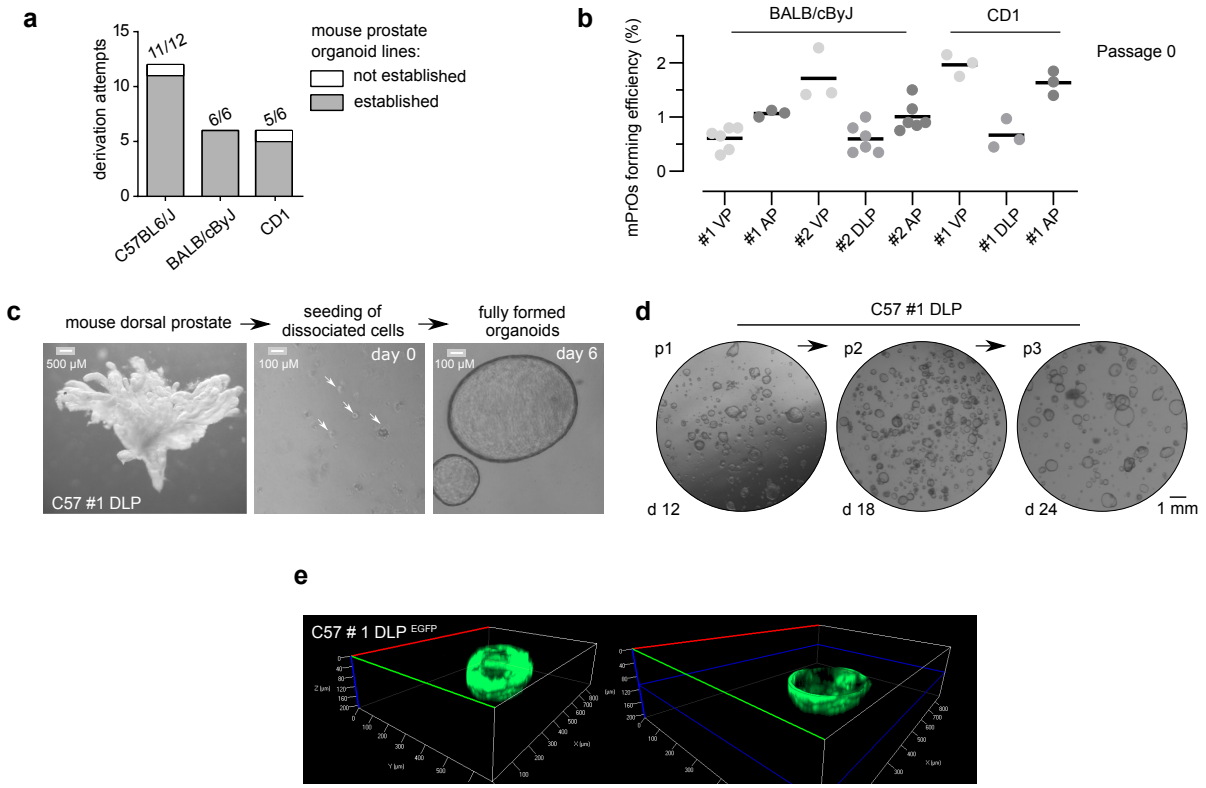

Establishment of a mouse prostate organoid biobank

a. Prostate organoid derivation rate from distinct mouse strains.

b. Mouse prostate organoid forming efficiency at derivation. Data points are shown with crossing line representing mean value.

c. Representative stereoscopic images at different stages of mouse prostate organoid derivation.

d. Representative stereoscopic images of mouse prostate organoid cultures during subsequent passages.

e. Representative 3D reconstruction of a fully formed mouse prostate organoid based on live epifluorescent microscopic analysis (1 µm section x 300 planes). On the right side, only the bottom half of the organoid is displayed.

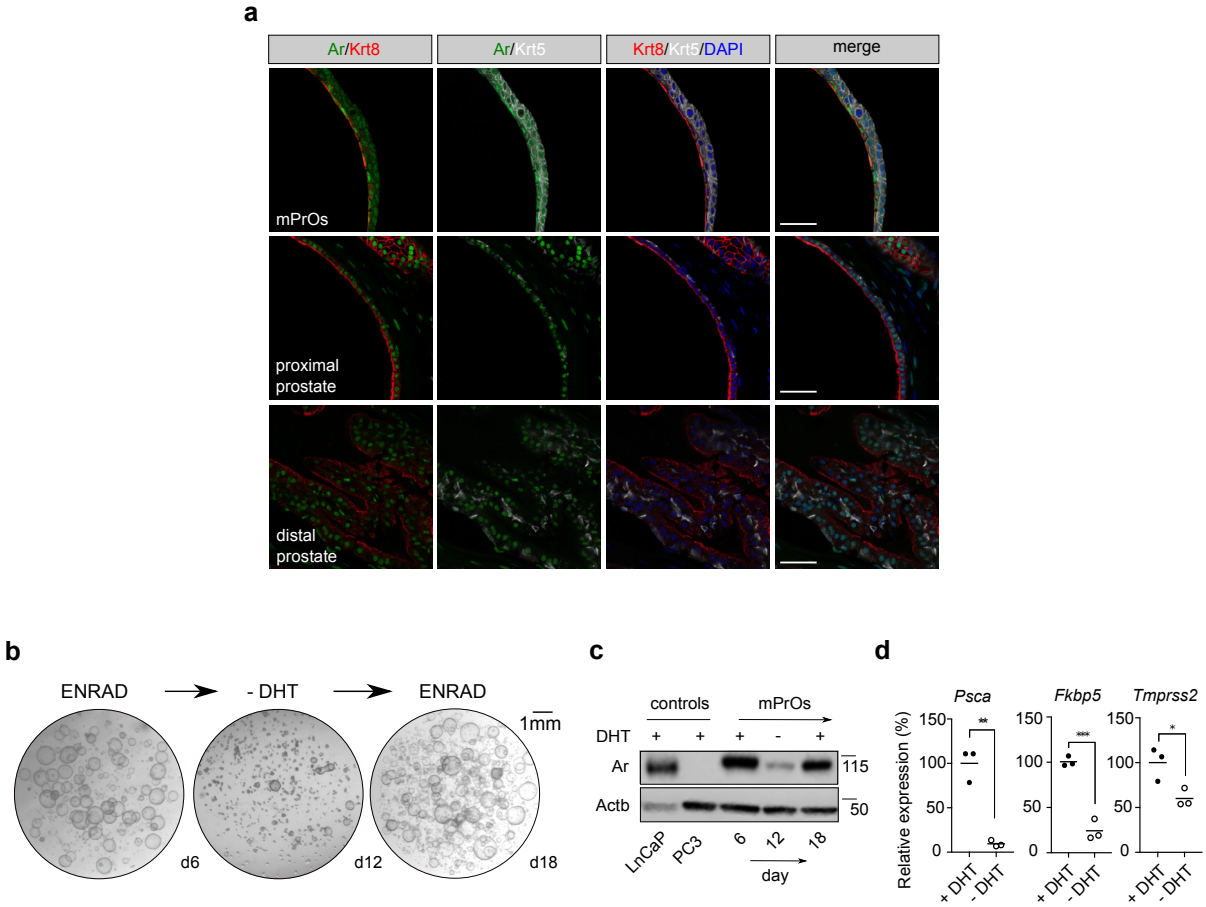

Mouse prostate organoids are dependent on androgen signalling for lumen formation - but not for survival

a. Immunofluorescence analysis for selected markers in mouse prostate tissue and organoid sections (scale bars = 50 µm).
b. Stereoscopic images of mouse prostate organoids experiencing transient dihydrotestosterone (DHT) removal (androgen cycling). Lumen formation necessitates androgen signaling.
c. Western blot analysis for Androgen receptor (Ar) expression in mouse prostate organoids experiencing androgen cycling, and control cell lines expressing (LnCaP) or not expressing (PC3) the receptor.
d. qRT-PCR mRNA expression analysis for selected androgen-responsive genes in the presence or absence of DHT. Data points are shown with crossing line representing mean value. Student's t-test, two-tailed, p-value * (<0.05), ** (<0.01), *** (<0.001).

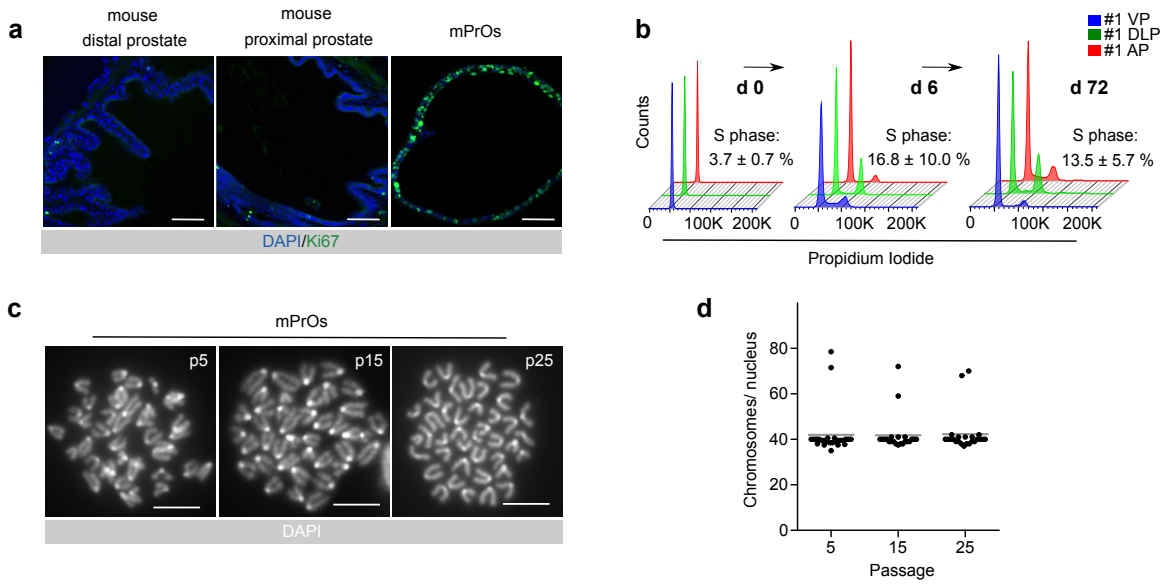

Low levels of genomic instability in fast cycling mouse prostate organoids

a. Immunofluorescence staining for Ki67 in mouse prostate tissue and organoid sections (scale bars = 50 µm)
b. Flow cytometry analysis for DNA content
c. Representative karyotypes (scale bars = 10 µm)
d. Quantification of karyotype analysis. Data points are shown with crossing line representing mean value.

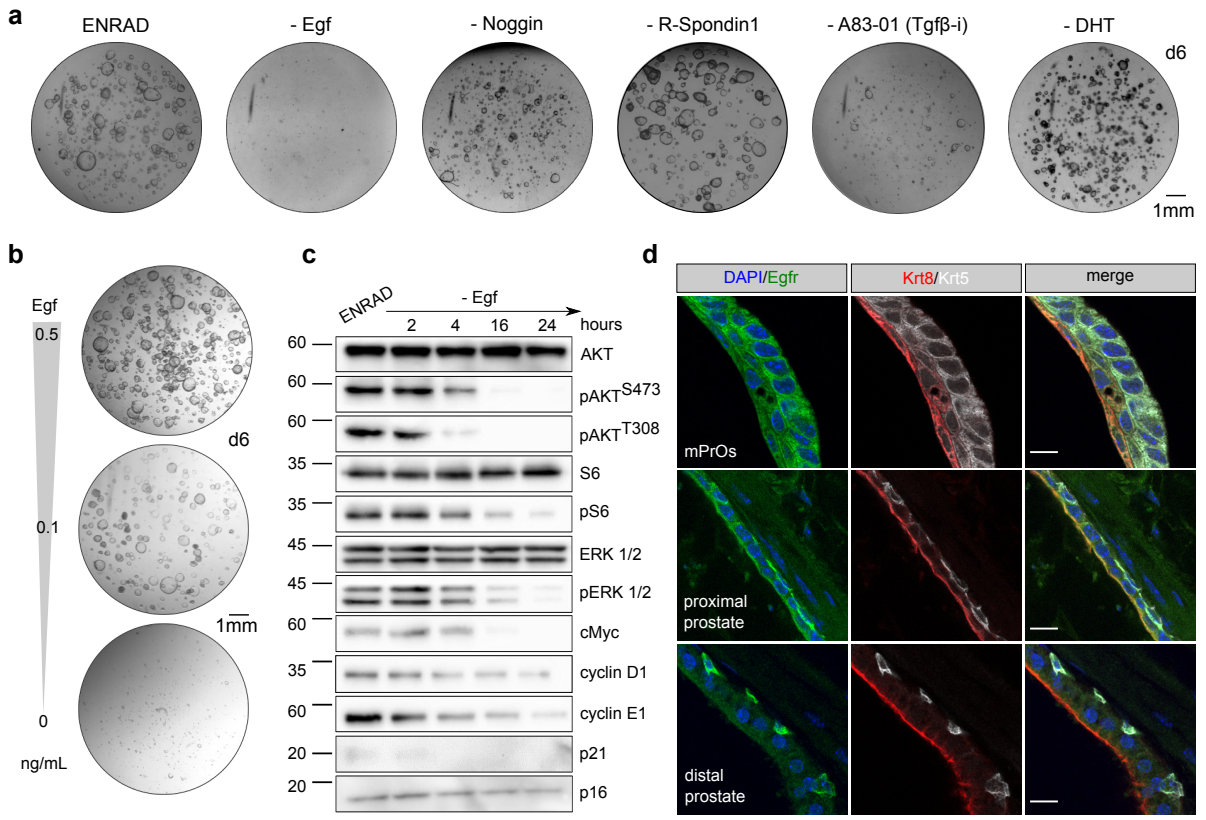

Mouse prostate organoids rely on Egf signalling for continuous proliferation

a. Representative stereoscopic images of mouse prostate organoid grown in complete medium (ENRAD) vs. medium depleted of individual growth factors/inhibitors. Mouse prostate organoids necessitate of both Egf and the Tgf-β inhibiitor A83-01 for continuous expansion. Within the period of observation, removal of Noggin or R-Spondin 1 has no clear consequence in culture. Please note that organoids failed to form a lumen in the absence of dihydrotestosterone (DHT).

b. Stereoscopic images of mouse prostate organoids cultured in the presence of reduced levels (0.5, 0.1 ng/mL) or in the absence of Egf.

c. Western blot analysis in mouse prostate organoids for selected signalling mediator and cell cycle regulator proteins.

d. Immunofluorescence analysis for selected markers in mouse prostate tissue and organoid sections (scale bars = 10 μm).

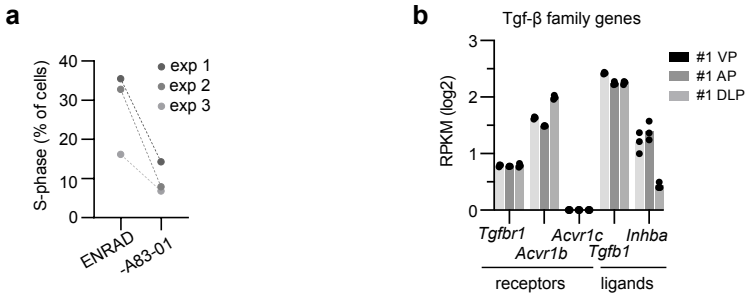

Inhibition of Tgf-β receptors is required for cell cycle progression in mouse prostate organoids

a. Quantification of cells undergoing S-phase based on flow cytometry (EdU *vs*. TO-PRO-3) in complete medium (ENRAD) or in the absence of A83-01 (24 hours). (Related to Fig 2a; n=3, individual data points are shown.)

b. mRNA expression levels for selected Tgf-β family receptors and ligands. Bulk-RNAseq analysis (n=3; individual data points are shown with bar graphs representing mean value).

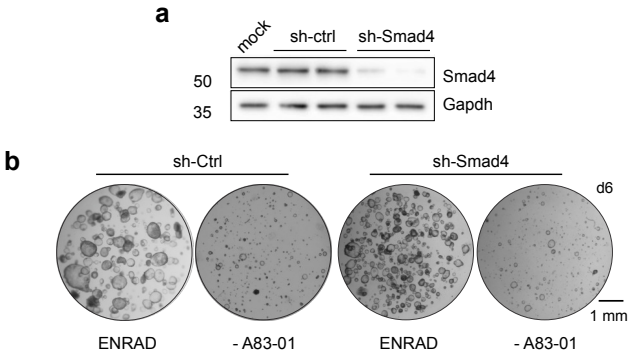

Canonical Smad signalling is dispensable for Tgf-β induced quiescence in prostate organoids

a. Western blot analysis for Smad4 in mouse prostate organoids upon short-hairpin RNA mediated knockdown (sh-Smad4) and in control conditions (sh-Ctrl).

b. Representative stereoscopic images of control (sh-Ctrl) and Smad4 knocked down (sh-Smad4) mouse prostate organoids in normal growth condition (ENRAD) and following A83-01 withdrawal (-A83-01).

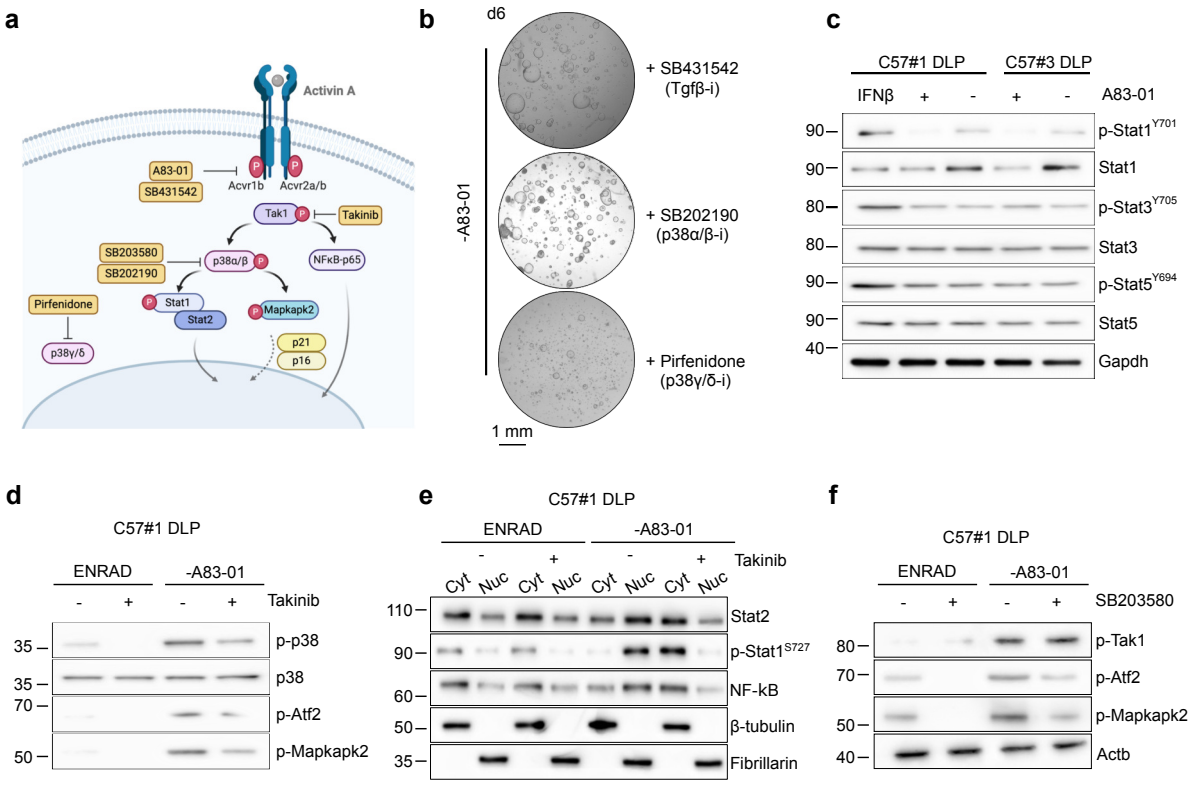

Tak1/p38 MAPK signalling activates immune- and stress-related pathways in prostate organoids

a. Schematic view of the non-canonical Activin A signalling pathwaty, including inhibitors used for the experiments described in this figure.

b. Representative stereoscopic images of mouse prostate organoids grown in the absence of A83-01 and in the presence of either SB431542 (Tgfβ-receptor inhibitor; 10 μM, 6 days), or SB202190 (p38α/β inhibitor; 10 μM, 6 days), or Pirfenidone (p38γ/δ inhibitor; 10 μM, 6 days).

c. Western blot analysis in mouse prostate organoids for canonical IFN signalling mediators upon acute A83-01 withdrawal (IFNβ; 50 ng/mL, 6 days).

d-f. Western blot analysis in mouse prostate organoids for key components of the non-canonical Tgf-β pathway and IFN signalling upon acute A83-01 withdrawal and concomitant inhibition of either Tak1 (Takinib; 5 μM, 24 hours) (**d**, **e**) or p38α/β (SB203580; 10 μM, 24 hours) (**f**).

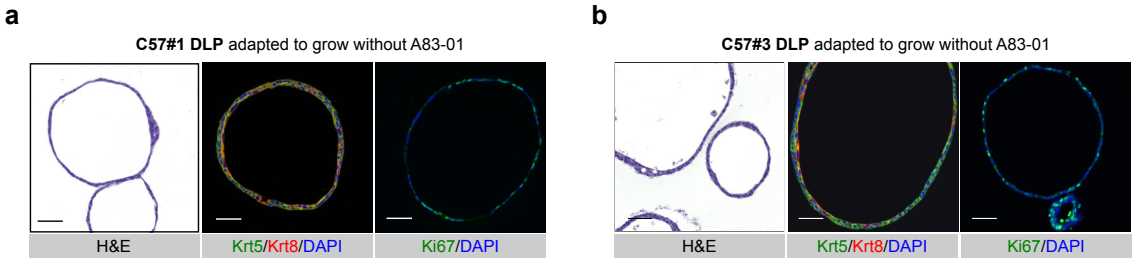

Mouse prostate organoids adapted to the absence of the Tgf-b receptor inhibitor A83-01 retain quasi-normal cellular identities and cytoarchitecture

a-b. Representative H&E and immunofluorescence analyses of C57#1 and C57#3 DLP mouse prostate organoids upon adaptation to A83-01 withdrawal (scale bar = 50 µm). Please note the adapted organoids retain a pattern of cytokeratins expression consistent with normal cellular identities, including basal, luminal P (lumP) and peri-uretheral (PrU)

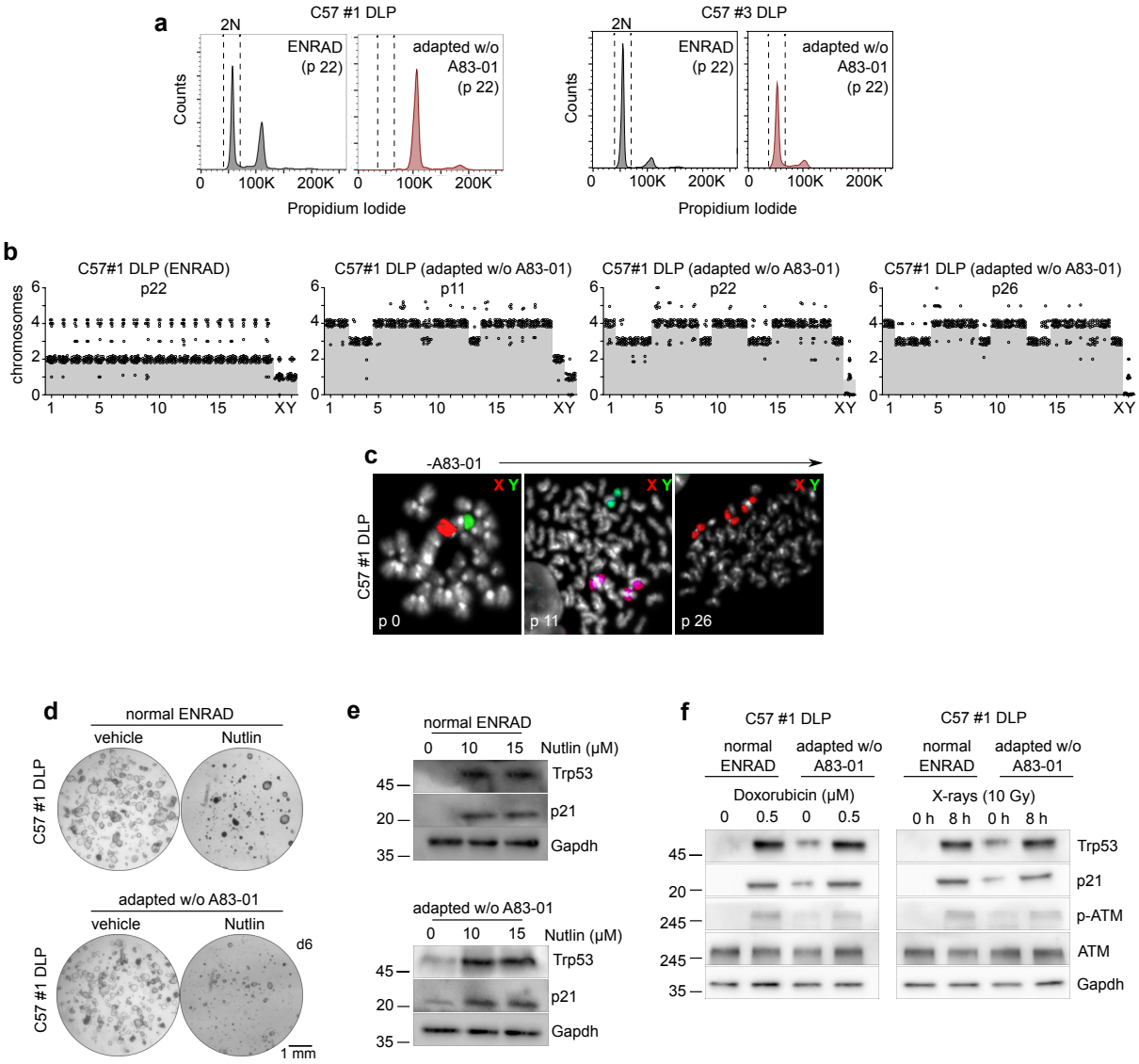

C57#1 DLP mouse prostate organoids adapted to the absence of A83-01 in culture display widespread genomic instability while retaining an intact p53 pathway

a. DNA content analysis in C57#1 DLP and C57#3 DLP mouse prostate organoid lines.
b. Quantification of spectral karyotype (SKY) longitudinal analysis in C57#1 DLP mouse prostate organoids undergoing adaptation to the absence of A83-01 in culture (related to Fig 3f). During adaptation, an early genome duplication event is observed followed by selective chromosome loss and gains, and leading to subtetraploidy.
c. Representative dual-colour FISH images for X and Y chromosomes in C57#1 DLP mouse prostate organoids during adaptation to the absence of A83-01 in culture. This analysis confirmed a progressive sex chromosome imbalance during adaptation.
d. Representative stereoscopic images of C57 #1 DLP mouse prostate organoids treated with Nutlin, or vehicle as control.
e. Western blot analysis of C57 #1 DLP mouse prostate organoids described in **d**.
f. Western blot analysis in C57 #1 DLP mouse prostate organoids treated with doxorubicin or X-rays. C57#1 DLP mouse prostate organoids retain a functional p53 pathway.

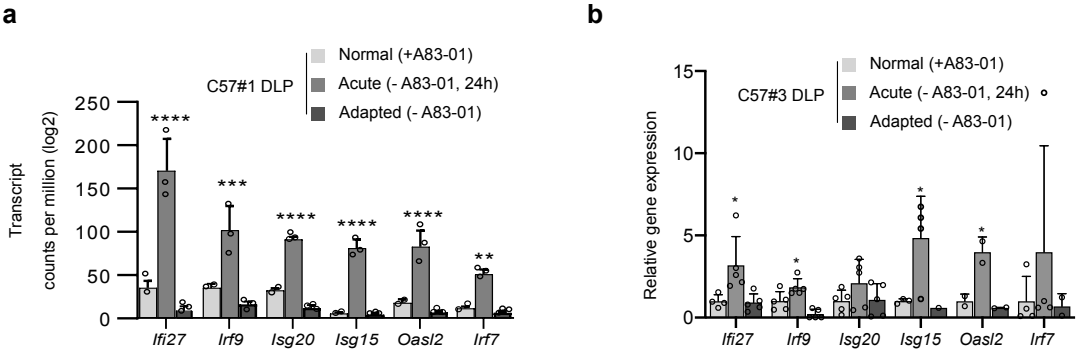

Non- canonical Activin A signalling regulates type-I interferon genes in mouse prostate organoids

a-b. mRNA expression levels for selected type-I IFN response genes in C57#1 and C57#3 DLP mouse prostate organoids cultured in complete medium (normal), upon acute A83-01 withdrawal (acute), and adapted to grow without A83-01 (adapted). Transcription of type-I interferon genes is enhanced upon A83-01 withdrawal and reduced upon adaptation (n=3, bulk-RNAseq analysis (a) or qPCR (b); individual data points are shown with bar graphs representing mean value and standard deviation; two-way ANOVA, Tukey's test, p-value * (<0.05), ** (<0.01), *** (<0.001), **** (<0.0001).

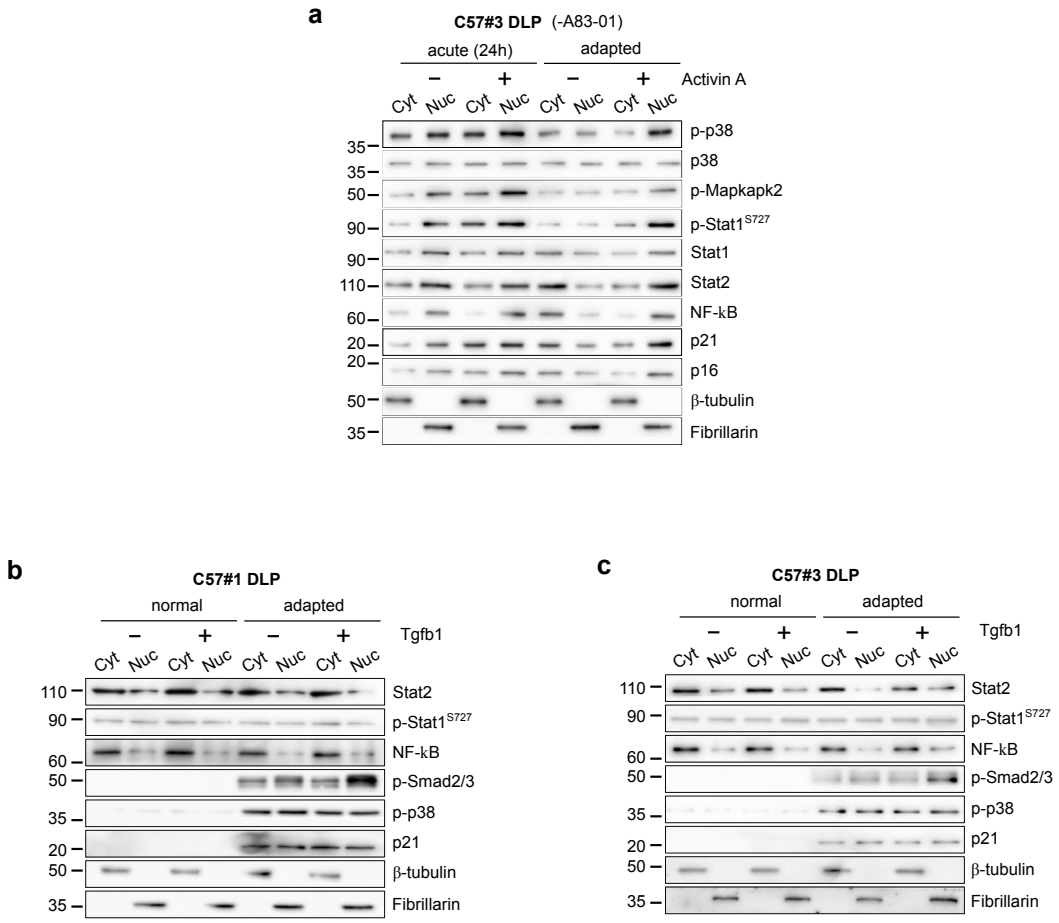

Restoration of Activin A signalling – not Tgb1 – leads to cytostasis in organoid lines (C57 #1 and #3) adapted to grow in the absence of A83-01.

a. Western blot analysis of C57#3 DLP mouse prostate organoid line upon acute removal (24 hours) or adapted to grow without A83-01, in the presence or absence of Activin A (50 ng/mL, 24 hours).

b. Western blot analysis of C57#1 DLP normal or adapted to grow without A83-01 mouse prostate organoid lines, in the presence or absence of Tgfb1 (500 ng/mL, 24 hours).

c. Western blot analysis of C57#3 DLP normal or adapted to grow without A83-01 mouse prostate organoid lines, in the presence or absence of Tgfb1 (500 ng/mL, 24 hours).

Supplementary Table 1: Growth factors and small molecules

Treatment	Catalogue #	Concentration
Activin A	R&D, 338-AC	50 ng/mL
Tgfb1	SinoBiol, 50698-M08H	500 ng/mL
Follistatin	PeproTech, 120-13	500 ng/mL
SB203580	Tocris, 1202	10 μM
SB202190	PeproTech, 1523072	10 μM
SB431542	Sigma Aldrich, S4317	10 μM
Ralimetinib*	Selleckchem, S1494	1 μM
Pirfenidone	Cayman, 13986	10 μM
Takinib	Sigma-Aldrich, SML2216	5 μM
IFNβ	SinoBiol, 50708-MCCH5	50 ng/mL

*Organoids were pre-treated with Ralimetinib (1 μM) for 24 hours before being seeded for the experiments.

Supplementary Table 2: Primary antibodies used for IF, IHC and flow cytometry

Antigen	Catalogue #	Dilution
Krt5	BioLegend, 905901	1:500
Krt8	Merk, MAB329	1:200
Krt7	Abcam, ab68459	1:250
Krt8/18	Abcam, ab53280	1:1000
Ki67	eBioscience, 14-5698-82	1:200
Egfr	Abcam, ab52894	1:200
Acvr1b	R&D Systems, AF1477	1:500
Ppp1r1b	Invitrogen, MA5-14968	1:400
Ar	Santa Cruz Biotech, SC-816	1:500
Cd24a	eBioscience, BMS17-0242-82	1:800
Sca-1	BioLegend, 122514	1:800

Supplementary Table 3: Primers used for end-point and quantitative PCR

Gene	Primers Sequence
Ifi27	*fw:* 5'-ggcttccattgtctccaaga-3'
	rv: 5'-accttcagtgctccaagtgc-3'
Isg20	*fw:* 5'-cttctgaaaggcaagctggt-3'
	*rv:*5'-tcttgtgtagcaggcgctta-3'
Irf9	*fw:* 5'-ctctttgttcagcgcctttg-3'
	rv-5'-tcccagaaatgtagggttgc-3'
Isg15	*fw:* 5'-gagctagagcctgcagcaat-3'
	rv: 5'-taagaccgtcctggagcact-3'
Oasl2	*fw:* 5'-ctccggttggtgaagttctg-3'
	rv: 5'-gtcgcggtagtttacgagga-3'
Irf7	*fw: 5'*-gaagaccaacttccgctgtg-3'
	rv: 5'-agcattgctgaggctcactt-3'
Trp63	*fw:* 5'-agaacggcgatggtacgaag-3'
	rv: 5'-tctcacgacctctcactggt-3'
Ar	*fw:* 5'-gccaggagtggtgtgtgccg-3'
	rv: 5'-aagttgcggaagccaggcaagg-3'
Tmprss2	*fw:* 5'-gccgcctccggagatttaag-3'
	rv: 5'-aggtgaccctgagttcaatgc-3'
Psca	*fw:* 5'-gctcactgcaaccatgaaga-3'
	rv: 5'-gctaagtaggtggccagcag-3'
Nkx3.1	*fw:* 5'-cggaccctaggagggactc-3'
	rv: 5'-cacctgagtgtgagagaaggc-3'
Mme	*fw:* 5'-ctccaacttctccccaatccc-3'
	rv: 5'-tcgagcagctgattttatgcagt-3'
Pbsn	*fw:* 5'-tgcacagtatgaagggagcat-3'
	rv: 5'-tccgtgtccatgatacgctg-3'
Fkbp5	*fw:* 5'-agccgggaagcctaagtttg-3'
	rv-5'-acttgcctcccttgaagtaca-3'
Tgm4	*fw:* 5'-ctagagtcttgacagggctgc-3'
	rv-5'-tggtactcggatgtgtggtg-3'
Sbp	*fw:* 5'-ccagattgtaccacaaaccctc-3'
	rv-5'-ccgtcctccagaaggaagtc-3'
Sdha	*fw:* 5'-tggtgagaacaagaaggcatca-3'
	rv: 5'-cgcctacaaccacagcatca-3'
Tbp	*fw:* 5'-cggtcgcgtcattttctccgc-3'
	rv: 5'-gtggggaggccaagccctga-3'
Actb	*fw:* 5'-atccagctcctagcacgcacg-3'
	rv: 5'-gtccccgctttgcgcaggtg-3'
Gapdh	*fw:* 5'-gagagtgtttcctcgtcccg-3'
	rv: 5'-actgtgccgttgaatttgcc-3'

Supplementary Table 4: Primary antibodies used for western blot

Antigen	Catalogue #	Dilution
β-Actin	Merk, A2228	1:2000
β-Tubulin	Santa Cruz Biotech, sc-5274	1:4000
Akt	CST, 9272	1:2000
Akt phosphoSer473	CST, 4060	1:1000
Akt phosphoThr308	CST, 9275	1:1000
Ar	Santa Cruz Biotech, sc-816	1:500
Atf2 anti-phosphoThr71	CST, 9221	1:1000
Atm	CST, 2873	1:1000
Atm phosphoSer1981	CST, 5883	1:1000
c-Myc	Abcam, ab32072	1:1000
Chk1	CST, 2360	1:1000
Chk1 phosphoSer35	CST, 2348	1:1000
Cyclin D1	Abcam, ab134175	1:1000
Cyclin E1	CST, 20808	1:1000
Erk	CST, 9102	1:1000
Erk phosphoThr202/Tyr204	CST, 4370	1:1000
Fibrillarin	Abcam, ab4566	1:500
Gapdh	Thermo Fisher, MA515738	1:4000
Krt5	BioLegend, 905901	1:500
Krt8/18	Abcam, ab53280	1:1000
Mapkapk2 phosphoThr334	CST, 3041	1:1000
p16	Abcam, ab211542	1:500
p21	Abcam, ab109520	1:500
p38	CST, 9212	1:1000
p38 phosphoThr180/Tyr182	CST, 9215	1:500
Smad2 phosphoSer465/467	CST, 8828	1:1000
Smad2/3	CST, 8685	1:1000
Smad4	Santa Cruz Biotech, sc-7966	1:1000
Stat1	BD Biosciences, 610186	1:1000
Stat1 phosphoSer727	CST, 9177	1:1000
Stat1 phosphoTyr701	CST, 9171	1:1000
Stat2	CST, 4597	1:1000
Stat3	CST, 9132	1:1000
Stat3 phosphoTyr705	CST, 9131	1:1000
Stat5	CST, 9358	1:1000
Stat5 phosphoTyr694	CST, 9359	1:1000
Tak1	CST, 5206	1:1000
Trp53	Abcam, ab26	1:500